Polysaccharide II Surface Anchoring, the Achilles' Heel of Clostridioides difficile

Jeanne Malet-Villemagne, Liang Yucheng, Laurent Evanno, Sandrine Denis-Quanquin, Jean-Emmanuel Hugonnet, Michel Arthur, Claire Janoir, Thomas Candela

Polysaccharide II surface anchoring, the Achilles' heel of *Clostridioides difficile.*

Jeanne Malet-Villemagne[a], Yucheng Liang[d], Laurent Evanno[b], Sandrine Denis-Quanquin[c], Jean-Emmanuel Hugonnet[d], Michel Arthur[d], Claire Janoir[a], Thomas Candela[a#]

[a] Université Paris-Saclay, INRAE, AgroParisTech, Micalis Institute, Jouy-en-Josas, France.

[b] Biomolécules: Conception, Isolement et Synthèse (BioCIS), Université Paris-Saclay, CNRS, Orsay, France.

[c] Laboratoire de Chimie de l'ENS Lyon, CNRS and Université de Lyon, Lyon, France.

[d] INSERM UMR-S 1138, Centre de Recherche des Cordeliers, Sorbonne Université, Université Paris Cité, Paris, France.

Running head: PSII anchoring of *C. difficile*

#Address correspondence to Thomas Candela: thomas.candela@universite-paris-saclay.fr

Word counts: 250 (abstract), 148 (importance), 3921 (text)

Abstract

Cell wall glycopolymers (CWPGs) in Gram-positive bacteria have been reported to be involved in several bacterial processes. These polymers, pillars for proteins and S-layer, are essential for the bacterial surface set-up, could be essential for growth, and, in pathogens, participate most often in virulence. CWGPs are covalently anchored to the peptidoglycan by Lcp proteins that belong to the LytR-CpsA-PSr family. This anchoring, important for growth, was reported as essential for some bacteria such as *Bacillus subtilis*, but the reason why CWGPs anchoring is essential remained unknown. We studied LcpA and LcpB of *Clostridioides difficile* (*C. difficile*) and showed that they have a redundant activity. To delete both *lcp* genes, we set up the first conditional-lethal mutant method in *C. difficile* and showed that polysaccharide II (PSII) anchoring at the bacterial surface is essential for *C. difficile* survival. In the conditional-lethal mutant, *C. difficile* morphology was impaired, suggesting that peptidoglycan synthesis was affected. Because Lcp proteins are transferring CWPGs from the C55-undecaprenyl phosphate, also needed in the peptidoglycan synthesis process, we assumed that there was a competition between the PSII and the peptidoglycan synthesis pathways. We confirmed that UDP-Mur*N*Ac-pentapeptide precursor was accumulated, showing that peptidoglycan synthesis was blocked. Our results provided an explanation for the essentiality of PSII anchoring in *C. difficile* and suggest that the essentiality of the anchoring of CWPGs in other bacteria can also be explained by the blocking of peptidoglycan synthesis. To conclude, our results suggest that Lcps are potential new targets to combat *C. difficile* infection.

Importance

Cell wall glycopolymers (CWGPs) in gram-positive bacteria have been reported to be involved in several bacterial processes. The CWGPs anchoring to the peptidoglycan is important for growth and virulence. We set up the first conditional-lethal mutant method in *C. difficile* to study LcpA and LcpB involved in the anchoring of the CWPGs to the peptidoglycan. This study offers new tools to reveal the role of essential genes in *C. difficile*. LcpA and LcpB activity was shown to be essential, suggesting that they are potential new targets to combat *C. difficile* infection. In this study, we also showed that there is a competition between the polysaccharide II synthesis pathway and the peptidoglycan synthesis that probably exists in other Gram-positive bacteria. A better understanding of these mechanisms allows us to define the Lcp proteins as a therapeutic target for a potential design of a novel antibiotic against pathogenic Gram-positive bacteria.

Introduction

In recent years, there has been an increasing interest in cell wall glycopolymers (CWGPs) in Gram-positive bacteria for their role in bacterial physiology and pathogenicity. These polymers represent up to 50% of the dry weight of the cell wall (1). CWGPs are covalently linked to peptidoglycan (PG). They support surface proteins (like Cwp in *Clostridioides difficile* or SLH in *Bacillus subtilis*) that are non-covalently anchored at the very end of CWGPs (2, 3). Most of them are essential and involved in cell division and cell shape maintenance (for review (4)). In pathogens, they are essential for virulence (5–11). They are therefore thought to be targets for the conception of new antimicrobial molecules (12, 13).

CWGPs anchoring is of major importance for the physiology of Gram-positive bacteria. This process was shown to be done by proteins belonging to the LytR-CpsA-PSr (LCP) family. Members of this protein family are widespread in the bacterial world as they were identified in eight different bacterial phyla (14). The Lcp enzymes transfer CWGPs from a lipid carrier, the C_{55}-undecaprenyl phosphate ($C_{55}P$) to the nascent or mature PG (15–19). Lcp proteins are therefore key players in bacterial surface assembly. In Gram-positive bacteria, several copies of *lcp* genes are often observed but the gene products can have distinct catalytic activities. For example, in *B. subtilis*, three Lcp proteins have been identified and one of them (TagU) has a stronger activity than the two others (20). In *M. tuberculosis*, the only Lcp is essential (21). Finally, in *Staphylococcus aureus* (*S. aureus*), LcpA is the main transferase of teichoic acids whereas LcpC is dedicated to the capsular polysaccharides transfer (19). The Lcp proteins are at least partially redundant in *B. subtilis* (22), *S. aureus* (23, 24), and *Streptococcus pneumoniae* (25, 26). Besides, the Lcp proteins are good targets for

specific inhibitors development because their soluble catalytic domain is extracellular (accessible to immune system cells) and they have no homologs in mammals (14). In *C. difficile*, Lcps were studied individually (27), but their redundancy and essentiality for survival have never been assessed experimentally.

Clostridioides difficile (previously known as *Clostridium difficile*) is a Gram-positive, motile, strictly anaerobic, and spore-forming enteric pathogen. *C. difficile* infections (CDIs) are a primary cause of nosocomial diarrhea and antibiotic-associated colitis (28). Besides, the incidence and the number of severe clinical forms have been increasing in recent years, due to emerging hypervirulent and antibiotic-resistant strains (including *C. difficile* ribotype 027) (29). Consequently, *C. difficile* is considered an urgent threat to public health by the Centers for Disease Control and prevention (30). Moreover, multiple resistance mechanisms to currently used antibiotics, often mediated by plasmid acquisition (31, 32), are observed and cause concerns about future treatment options for CDI management. Therefore, developing new strategies and discovering new bacterial targets is necessary.

In *C. difficile*, three CWPGs have been identified: two teichoic acids (TA) anchored in the peptidoglycan (polysaccharides I and II, (33)) and one lipoteichoic acid (LTA) anchored directly in the membrane (34). Only the polysaccharide II (PSII) and the LTA are conserved among *C. difficile* strains. All the biosynthesis genes of these glycopolymers are encoded in a single locus of the chromosome. All the genes predicted to encode enzymes involved in PSII synthesis are reported to be essential for bacterial survival (3, 35), but surprisingly not *lcpA* and *lcpB* genes encoding PSII anchoring proteins (27). Note that Cwp proteins, including the S-layer protein SlpA, are non-covalently linked to the PSII (3).

In this study, we focused on PSII. Its biosynthesis is predicted to be initiated by the transferase CD2783, transferring the first sugar unit (UDP-Glucose) on the $C_{55}P$ lipid carrier. Then, several cytoplasmic glycosyltransferases catalyze the transfer of sugar units on the chain. When finished, the chain is flipped outside the cell by the flippase MviN (27) and transferred to the pre-existing chains to form a $C_{55}P$-polymerized PSII molecule. PSII is then transferred from the lipid carrier to the PG by LcpA and LcpB (27). In this work, we studied the two Lcps of *C. difficile* to evaluate the importance of a correct polysaccharide anchoring in the physiology of the bacterium. We wanted to determine if the *lcp* genes were essential for survival.

Results

Construction of *lcp* single mutants

To facilitate the screen of the allelic exchange technique in *C. difficile* (36), we decided to replace the open reading frame of *lcpA* and *lcpB* with the open reading frame of the *catP* gene expressing the thiamphenicol resistance. To that aim, we constructed the pJV10 vector that harbors an *ermB* gene (Figure S1) conferring erythromycin resistance. In the genome of the 630 strain, two copies of the *ermB* gene are found. In contrast, the 630Δ*erm* harbors only one *ermB* gene (37), which is usually not expressed. However, we were unable to conjugate the pJV10 plasmid in the 630Δ*erm* that became, in these conditions, resistant to erythromycin, probably because the remaining *ermB* gene was sufficiently expressed during the conjugation process. Therefore, we chose to construct a “true” 630Δ*erm* by deleting both *ermB* genes directly from the clinical 630 strain and obtained the JMV1 strain.

We first deleted *lcpA* and *lcpB* separately in the JMV1 strain using the allelic exchange method (36). Thanks to the presence of the *catP* gene, after the selection of the first crossing over (36), a simple restreak on a petri dish in the presence of thiamphenicol allows the identification of potential mutant clones. The JMV3 (Δ*lcpA*) strain was easily obtained (21 mutant clones were thiamphenicol resistant out of 25) whereas the JMV4 (Δ*lcpB*) strain was quite hard to get (3 mutant clones were thiamphenicol resistant out of 187), suggesting that *lcpB* plays an important role for *C. difficile* growth.

lcpA and *lcpB* are redundant

We first confirmed that the *lcpB* mutant (JMV4) showed a growth defect (Figure S2). Then, we observed the morphology of the mutant cells in classical optic microscopy (Figure 1A) and measured the cell length and width (Figure 1C and 1D), allowing us to determine a percentage of "normal morphology" (Figure 1B). Contrary to the Δ*lcpA* mutant bacteria (JMV3) whose morphology is normal, almost 35% of the Δ*lcpB* (JMV4) cells were curved or inflated (Figures 1 and S3). Cells were also significantly longer and thicker than the JMV1 cells (Figures 1C and 1D). These observed morphological and growth defects in the absence of *lcpB* confirmed the previous results obtained by Vedantam *et al.* (27) and suggest that LcpB plays a major role in anchoring the PSII to the peptidoglycan.

Besides, we observed that bacterial morphology and growth were restored in the strains JMV4 + pMEZ12 (complementation plasmid bearing *lcpA*, named thereafter p*lcpA* for simplification) and JMV4 + pJV21 (complementation plasmid bearing *lcpB*, named thereafter p*lcpB* for simplification), as shown in Figures 1A and S2. Indeed, the abnormal cell ratio was reduced to 4% and 6% when complementation with *lcpA* or *lcpB* was introduced (Figure 1B). These results suggest that LcpA can compensate for the absence of LcpB in anchoring the PSII to the peptidoglycan and that both Lcp proteins have redundant functions in *C. difficile*.

Considering the absence of phenotype in the JMV3 strain, we wondered if *lcpA* was expressed and we assessed the expression of *lcpA* and *lcpB* by a measurement of the promoter activity (by beta-glucuronidase assay). As shown in Figures 2A and 2B, *lcpA* and *lcpB* had constitutive expression, respectively with a mean of 230 and 35 Miller units, but *lcpA* is transcribed at a higher level than *lcpB*. This result suggested, that even if transcribed at a low level, *lcpB* is important for cell growth and morphology.

The Δ*lcpA* (JMV3) and Δ*lcpB* (JMV4) mutant strains present a normal surface protein profile but an altered PSII layer

Because Cwp proteins are non-covalently anchored to the PSII, we analyzed the S-layer content (Figure S4). We found no differences between the CWP proteins of the parental strain and the single mutants. To assess the presence of PSII at the bacterial surface, we purified the PSII, checked that it was non-contaminated with LTA by NMR (Figure S5), and coupled it with BSA. After immunization, we obtained specific antibodies able to recognize the PSII (Figure S6). Using a super-resolution microscope, the JMV1 parental strain showed a homogenous and continuous layer of PSII along the bacterium. In contrast, both JMV3 and JMV4 mutant strains showed an altered PSII layer (Figure 3). The JMV3 cells presented a holed layer of PSII. The JMV4 mutant strain presented a smooth PSII layer. The alteration of the PSII deposition at the surface was present in both mutants but the PSII layer was differently altered in the JMV3 and JMV4 strains, suggesting that even though redundant in activity, LcpA and LcpB have slightly different roles in PSII anchoring at the bacterial surface.

PSII anchoring is essential for *C. difficile* survival

Once the single mutants were obtained and their phenotypes confirmed, we tried to get a double mutant strain to assess the essentiality of the PSII anchoring for *C. difficile* survival. The first strategy was to use our improved allelic exchange method using the pJV13 plasmid and the *C. difficile* JMV1 strain. Despite the facilitated screening of mutants, we failed to isolate a double *lcp* mutant over the 450 clones tested. This result

187 suggested that deleting both *lcpA* and *lcpB* genes was not possible, maybe because
188 ofthe essentiality of bothLcpA and LcpB.
189 To assess the essentiality of *lcp* genes in *C. difficile*, we elaborated a new strategy
190 based on the construction of a conditional-lethal mutant (Figure S7). The first step was
191 to insert an extra copy of *lcpB* under the control of a P_{tet} promotor in the *ermB* locus of
192 the 630, to mimic the JMV1 strain by removing both *ermB* genes, giving rise to the JMV2
193 strain. The second step was to perform the deletion of both *lcpA* and *lcpB* in the JMV2
194 strain using pJV13 plasmid in the presence of 100 $ng.mL^{-1}$ of anhydrotetracycline (ATc).
195 We obtained the conditional-lethal mutant strain JMV6 that was not able to grow without
196 induction of the additional copy of *lcpB* (Figures 4A and S8). To confirm this phenotype,
197 conditional-lethal mutant strain (JMV6) was grown in the presence of 10 or 50 $ng.mL^{-1}$ of
198 ATc and then plated on a Petri dish with no or up to 250 $ng.mL^{-1}$ (Figure 4A). No growth
199 was observed on plates at 10 $ng.mL^{-1}$ ATc or less, showing that the presence of at least
200 one *lcp* is essential for *C. difficile* growth. In liquid culture, conditional-lethal mutant strain
201 (JMV6) in the presence of 10 $ng.mL^{-1}$ had an impaired growth that was restored by
202 adding 50 $ng.mL^{-1}$ of ATc (Figure 4B). Without ATc, growth was restored when *lcpA* was
203 present (on *plcpA* plasmid) confirming the redundancy of Lcp activity. We also assessed
204 the morphology using microscopy and confirmed that the conditional-lethal mutant strain
205 (JMV6) grown with 10 $ng.mL^{-1}$ of ATc had a marked phenotype with ellipsoid cells
206 shorter and thicker than the JMV1 cells (Figure 5). In the presence of 50 $ng.mL^{-1}$ of ATc,
207 some bacilli were curved and long but the rod shape was restored with comparable cell
208 width and increased cell length compared to JMV1 cells (Figure 5). Finally, the addition
209 of p*lcpA* or p*lcpB* fully restored the bacterial shape, similarly to the controls (JMV1 and
210 JMV2 strains). Our results showed that the absence of *lcpA* and *lcpB* is lethal for *C.*

211 *difficile* and suggested that PSII anchoring is essential for *C. difficile* growth. In addition,
212 this result suggested that only *lcpA* and *lcpB* are involved in PSII anchoring.
213
214 ## PSII remains at the bacterial surface in the JMV6 strain
215 To analyze the localization of PSII at the bacterial surface when its anchoring is impaired
216 due to the limitation of LcpA and LcpB, the conditional-lethal mutant strain (JMV6) was
217 cultured with 10 ng.mL^{-1} or 50 ng.mL^{-1} of ATc (Figure 6). We used the JMV2 strain as a
218 control, which has a second copy of *lcpB* (P_{tet}-*lcpB* copy at the *ermB* locus). This strain
219 has a similar phenotype to the JMV1 strain confirming that overexpression of *lcpB*, due
220 to the induction of the second copy, does not affect PSII anchoring and bacterial
221 morphology. In the conditional-lethal mutant strain (JMV6), we confirmed that a low
222 induction of *lcpB* (10 ng.mL^{-1} of ATc) leads to ellipsoid cells. The rod shape was restored
223 in the presence of 50 ng.mL^{-1} of ATc with or without *lcpA*. Moreover, PSII was still
224 localized at the bacterial surface of the JMV6 strain in the presence of 10 ng.mL^{-1} of ATc
225 (Figure 6, JMV6 (ATc 10)). This result was surprising because, according to the previous
226 study of Chu *et al*. (27), PSII was expected to be found in the supernatant fraction. Our
227 results suggested that the PSII, after its synthesis was still anchored to its lipid carrier at
228 the plasmic membrane, in accordance with the models (20, 27).
229
230 ## Part of the surface PSII and Cwp proteins is released in the JMV6 strain
231 To assess the impact of a defect of PSII anchoring to PG, we analyzed the presence of
232 PSII at the bacterial surface and in the supernatant by dot blot analysis (Figure 7). In the
233 JMV1 parental strain and the JMV2 control strain (P_{tet}-*lcpB*), the PSII was found in the

bacterial fraction (pellet), suggesting that it was only associated with the bacterial surface. The same result was observed for the single *lcp* mutant strains JMV3 and JMV4. Conversely, in the conditional-lethal *lcp* mutant (JMV6) with 10 ng.mL^{-1} of ATc, PSII was found at the bacterial surface and released in the culture supernatant. This release of PSII is decreased in the presence of 50 ng.mL^{-1} of ATc. The phenotype is completely restored in the conditional-lethal mutant strain (JMV6) in the presence of *lcpA* and 50 ng.mL^{-1} of ATc.

Because the PSII was released in the supernatant, we assessed whether the Cwp proteins, which are non-covalently linked to the PSII, were also found in the supernatant. We showed that the Cwp amount was decreased at the bacterial surface of the conditional-lethal mutant strain (JMV6) in the presence of 10 ng.mL^{-1} ATc induction, in comparison with the JMV1, JMV2, and JMV6+*lcpA* strains (Figure 8A). Cwp proteins of the conditional-lethal mutant strain (JMV6) strain in the presence of 10 ng.mL^{-1} were found in the supernatant. In comparison, in the presence of 50 ng.mL^{-1}, Cwp proteins from the JMV6 strain were more abundant at the bacterial surface. To further characterize which proteins were concerned, we performed a western blot analysis. These analyses allowed us to identify two proteins of the Cwp family, Cwp66 and SlpA, in the supernatant of the conditional-lethal mutant strain (JMV6) strain (Figures 8D and 8F). Accordingly, Cwp66 was absent from the surface protein extracts (Figure 8C) and SlpA was found in a lower quantity than in other strains (Figure 8E). It is to note that SlpA precursor (uncleaved) was found in the conditional-lethal mutant strain (JMV6), suggesting a maturation defect. We analyzed the autolysis profile of all strains to investigate why the PSII and the Cwp proteins were found in the supernatant (Figure 9). We found that the single *lcp* mutants JMV3 and JMV4 autolyzed more rapidly than the

parental strain (Figure 9A) and that this phenotype was absent when they were complemented with either p*lcpA* or p*lcpB*. The conditional-lethal mutant JMV6 autolyzed also more rapidly than the JMV1 strain (Figure 9B). Again, the impaired phenotype was fully restored in the presence of 50 ng.mL-1 of ATc and *lcpA*. These results suggested that the conditional-lethal mutant strain (JMV6) is lysing more rapidly than the parental strain, explaining the partial release of the PSII into the culture supernatant.

Cytoplasmic PG precursors accumulate in response to impaired PSII anchoring to PG

Because the PSII is attached to the $C_{55}P$ carrier during its biosynthesis and until an Lcp protein anchors it to the peptidoglycan, we hypothesized that the PSII transfer impairment from the $C_{55}P$ carrier to the peptidoglycan may limit the availability of this lipid carrier for peptidoglycan synthesis. The extraction of cytoplasmic peptidoglycan precursors was performed for JMV1, conditional-lethal mutant strain JMV6 (10 ng.mL^{-1} ATc), and conditional-lethal mutant strain JMV6 + p*lcpA* (50 ng.mL^{-1} ATc) (Figure 10). In the JMV1 strain, only peak 1 was found (Figure 10A). In the two other tested strains (Figures 10B and 10C), peak 1 and peak 2 were found. Mass spectrometry analyses (Figure 10D) indicated that the precursor in peak 1 was UDP-Mur*N*Ac-pentapeptide. Analysis of the precursor in peak 2 by tandem mass spectrometry indicated that it differed from UDP-Mur*N*Ac-pentapeptide by the amidation of the side-chain carboxyl of the diaminopimelyl (DAP) residue located at the 3rd position of the pentapeptide stem. This amidation, attributed to AsnB, was only reported once, when *C. difficile* was grown in the presence of vancomycin at a sublethal concentration (38). A third peak (Figure

281 10B and C) was not identified. UDP-Mur*N*Ac-pentapeptide was 21-fold more abundant
282 in JMV6 grown in the presence of 10 ng.mL^{-1} of ATc than in the parental JMV1 strain.
283 The accumulation of UDP-Mur*N*Ac-pentapeptide was less abundant (6 fold instead of 21
284 fold) in the JMV6 + p*lcpA* strain, in the presence of 50 ng.mL^{-1} of ATc. These results
285 establish that impaired PSII anchoring to peptidoglycan results in the accumulation of
286 the UDP-Mur*N*Ac-pentapeptide peptidoglycan precursor. This accumulation is likely to
287 result from a limited availability of the C_{55}P lipid carrier for peptidoglycan synthesis due
288 to its sequestration in lipid-linked PSII precursors.
289

290 **Discussion**

291 In this study, we characterized LcpA and LcpB as responsible for PSII anchoring
292 to *C. difficile* PG. In addition, we showed that the activity of these proteins is essential for
293 the viability of *C. difficile* probably because of an interference with the PG synthesis.

294 In well-studied Gram-positive models like *B. subtilis*, *S. pneumoniae,* and *S.*
295 *aureus*, *lcp* genes are found in multiple copies in the genome and are at least partially
296 redundant (22–26). Our study confirmed that growth of a *lcpB* mutant strain is
297 associated with morphological defects, contrary to a *lcpA* mutant strain (27). *lcpB*
298 appears then to be more important than *lcpA*, yet *lcpB* is expressed at a lower level than
299 *lcpA*. The morphological and growth defects of the *lcpB* mutant were restored by
300 overexpression of *lcpA*. The overexpression may localize LcpA differently than in the
301 parental strain, allowing the complementation by compensating the absence of LcpB at
302 the bacterial surface and suggests that LcpA and LcpB have partially redundant
303 functions. Similarly, in other bacteria, yet redundant in activity, one Lcp has a

predominant role, and its absence impacts bacterial physiology more than the others (22, 39, 40).. Our immunofluorescence study (Figure 3) showed that the PSII layer is altered in both single mutants but differently, suggesting that these distinct phenotypes can be due to a different localization of the two Lcps at the surface. It is to note that LcpB is predicted to have a transmembrane domain and LcpA only has a signal peptide domain (https://www.ebi.ac.uk/interpro/), suggesting that LcpB is localized at the membrane and LcpA is secreted. Since the PSII is linked to the $C_{55}P$ at the membrane, a membranous Lcp (LcpB in *C. difficile*) may be more efficient in transferring it from the $C_{55}P$ to PG. In contrast, LcpA should be less efficient because of its lack of an N-terminal transmembrane domain which is untypical among Lcp proteins, since they usually have at least a transmembrane domain (14).

Lcp proteins are phosphotransferases according to Kawai *et al.* (22) or peptidoglycan-glycopolymer ligase according to Schaefer *et al.* (40). However, in *lcp* mutants of *S. aureus* and *B. subtilis*, CWGPs were found to be released (22, 23, 27). There is a discrepancy between these data and the theoretical CWGP synthesis and transfer of the CWGPs from the $C_{55}P$ to the PG. This was explained in *S. aureus* by the activity of CapA1 that catalyzes the cleavage of the pyrophosphate linkage between the CWGP and the $C_{55}P$, releasing the CWGP into the supernatant in the absence of Lcp proteins. In contrast, in *S. pneumoniae* (26) and our study, we reported that the CWGPs were found both in the supernatant and at the bacterial surface. In our work, it is difficult to know whether this PSII localization is due to the presence of a low level of LcpB (JMV6 in the presence of 10 $ng.mL^{-1}$ of ATc) or if PSII is still anchored to $C_{55}P$ carrier at the surface. In *C. difficile*, one gene encodes a putative protein similar to that of CapA1

from *S. aureus* (CD630_11190, 19% of identity and 45% of similarity) and none was found in the *S. pneumoniae* R6 genome. The CD630-11190 putative lipoprotein may have another function than CapA1, but we can't exclude that the observed release of PSII into the supernatant may be due to this protein, together with the observed bacterial lysis (Figure 9).

Additionally, we showed that PSII release in the conditional-lethal strain was associated with the release of the Cwp66 and SlpA surface proteins in the supernatant. Indeed, we were able to detect SlpA at the bacterial surface which is the most abundant surface protein in *C. difficile*, but not Cwp66, suggesting that most of the Cwp proteins are not localized at the bacterial surface anymore. In parallel, we observed that SlpA was only partially matured in the JMV6 strain, suggesting that Cwp84 was not efficient in its cleavage. This defect in SlpA cleavage may be due to the Cwp84 localization that was suggested to be first active when positioned at the surface, then released after an auto maturation, and finally fully active and reassociated to the bacterial surface (41). This last step may be missing due to a probable association with the released PSII instead of the bacterial surface, explaining the partial defect in SlpA cleavage.

Blocking indirectly the recycling of $C_{55}P$, for example with cell wall synthesis inhibitors (such as bacitracin and vancomycin), leads to an accumulation of UDP-Mur*N*Ac-pentapeptide in the cytoplasm and then bacterial death (42). Because the PSII is predicted to be anchored on the $C_{55}P$ lipid carrier during its biosynthesis (3, 27) and until it is transferred by Lcp proteins to the PG (19), we hypothesized that an impairment in PSII anchoring could lead to a blocking of peptidoglycan biosynthesis through a competition between the $C_{55}P$ linked PSII and the synthesis of lipid II that requires free

$C_{55}P$. Our results suggest that the sequestration of $C_{55}P$-linked PSII blocks the transfer of the UDP-Mur*N*Ac-pentapeptide to free $C_{55}P$, leading to its accumulation in the cytoplasm. During this accumulation, the UDP-Mur*N*Ac-pentapeptide is amidated (Figure 10). This amidation of a peptidoglycan precursor was already observed and mediated by AsnB in *C. difficile*, but only in the presence of vancomycin (38). As vancomycin also targets lipid II, we can hypothesize that the accumulation of UDP-Mur*N*Ac-pentapeptide may induce the expression of *asnB* leading to the amidation of peptidoglycan precursors.

UDP-Mur*N*Ac-pentapeptide accumulation suggested that the PG synthesis is blocked and explained the essentiality of Lcp activity in *C. difficile*. In *B. subtilis*, CWGPs are dispensable for cell viability (43), but the absence of the three Lcps is lethal (22). Similarly, in *Mycobacterium tuberculosis*, Lcp1, the unique Lcp, was shown to be essential (44). In other bacterial species, this essentiality was not reported, but the absence of Lcp led to defects in growth, morphology, and virulence (23, 40, 45). Our results confirmed the importance of the Lcp proteins in bacterial cell wall organization and their essentiality for bacterial physiology and fitness. Since Lcp proteins are mainly found in Gram-positive and especially in pathogens, they are very good targets for the research of a new class of antibacterial drugs to counteract the emergence of multidrug-resistant bacteria.

Materials and methods

Bacterial strains and growth conditions

The strains used and constructed in this study are listed in Table 1. All *C. difficile* strains of this study are isogenic derivatives of the clinical 630 strain (46). *C. difficile* was grown in a Brain-Heart Infusion medium (BHI, BD Difco) at 37°C in anaerobic conditions (Jacomex, 5% H_2 - 5% CO_2 - 90% N_2). When needed, BHI was supplemented with 1% defibrinated horse blood, thiamphenicol (Th, 7.5 µg.mL^{-1}), aztreonam (Az, 16 µg.mL^{-1}, used to kill parental *E. coli* during the conjugation process), or erythromycin (Er, 5 µg.mL^{-1}). Anhydrotetracycline (ATc) was used to induce the P_{tet} promoter (concentration from 5 to 250 ng.mL^{-1}). Growth curves were obtained using a SpectraMax plate reader (Molecular devices). *Escherichia coli* was grown aerobically in LB medium at 37°C, supplemented when needed with ampicillin (Amp, 100 µg.mL^{-1}), chloramphenicol (Cm, 25 µg.mL^{-1}), kanamycin (Kn, 40 µg.mL^{-1}), spectinomycin (Spec, 100 µg.mL^{-1}) or erythromycin (Er, 150 µg.mL^{-1}).

Molecular biology

According to the manufacturer's instructions, the plasmid extractions, gel extraction, and PCR purifications were achieved using the Omega E.Z.N.A Plasmid DNA Mini Kit, Gel extraction Kit, and Cycle Pure Kit. PCRs were carried out using high-fidelity Phusion DNA polymerase for gene amplification on genomic DNA and mutant screening of *C. difficile*. In contrast, the Taq DNA polymerase was used for screening steps in *E. coli*.

Construction of plasmids

A list of plasmids and primers used in this study can be found in Tables 1 (plasmids), S1, and S2 (primers). The construction of all plasmids is detailed in Text S1. The plasmids used in this study were constructed using either the Gibson assembly protocol from NEB (47) or the Golden Gate assembly from NEB (48, 49) cloning techniques. For Golden Gate assembly, the primers were designed using the NEB Builder® assembly tool.

Mutant strains construction

Plasmids were transferred from *E. coli* HB101 (pRK24) to *C. difficile* via heterogramic conjugation (between *E. coli* and *C. difficile*), following the previously described protocol (50). The single and double cross-over events were screened based on the pseudo-suicide plasmid pMSR following the appropriate protocol described by Peltier (36), with some modifications. As we replace the ORFs with a *catP* gene, a first quick screen for the second crossing-over event is done by restreaking clones on BHI supplemented with a thiamphenicol agar plate. Then, only Th^R clones are checked by PCR using appropriate primers (Table S2).

Construction of JMV1, JMV3, and JMV4 strains

The JMV1 strain is an Δ*ermB* region derivative of the clinical 630 strain. The deletion was made by replacing the complete *ermB* region [genes CD630_20100 (*ermB*), CD630_20091, CD630_20090, CD630_20080, CD630_20071, CD630_20070 (*ermB*)] with a spectinomycin resistance gene. This replacement was made by allelic exchange technique (36) using the pJV8 plasmid.

The single *lcp* mutants JMV3 and JMV4 are derivatives of the JMV1 strain, where the ORF was replaced with a thiamphenicol resistance gene. The deletion of CD630_27650 (*lcpA*) and CD630_27660 (*lcpB*) was made by allelic exchange using respectively deletion plasmids pJV11 and pJV12. The mutants were PCR-verified using the primers couples JV85/JV90, JV86/JV91 for JMV3 mutant, and JV88/JV90, JV87/JV91 for JMV4 strain (Table S2).

Conditional-lethal mutant construction

The insertion of the P_{tet}-*lcpB* in the *erm* locus was made using the pJV27 plasmid and the resulting strain JMV2 was PCR-verified using the JV99/JV100 primers. Then, the deletion of both *lcp* genes was made using the pJV13 plasmid and the use of 100 $ng.mL^{-1}$ of ATc, giving rise to the conditional-lethal mutant strain JMV6, which can be PCR-checked using primers JV85/JV90 and JV91/JV87 (Table 2).

Beta-glucuronidase assay

The beta-glucuronidase assay was performed as described in Ammam *et al.*, 2020 (38).

Growth and autolysis curves

Growth and autolysis curves were performed using the SpectraMax® plate reader. To ensure anaerobic conditions, the 96-wells plates were filmed with an adhesive film in the anaerobic chamber. The cultures were launched in BHI at an approximate optical density of 0.1 from overnight pre-culture of different strains. Growth and autolysis curves were performed at 37°C.

Cwp proteins and supernatant proteins extractions

Cwp proteins were isolated from intact *C. difficile* bacteria using low-pH glycine as described previously by Fagan *et al.* (51). The optical density was systematically adjusted to 1 for all strains before protein extraction. Supernatant proteins fraction was obtained by harvesting bacteria (20,000 x *g*, 15 min, 4 °C) from overnight cultures previously adjusted to an optical density (600 nm) of 1, and then precipitated with trichloroacetic acid 10% (on ice, 4 hours). The pellet is finally resuspended in Tris 50 mM pH 7.4.

Preparation of antigens and antibodies against PSII and SlpA

Surface polysaccharide II was isolated using the protocol of Cox (52). The detection of glycopolymers in fPLC fractions was accomplished by the phenol-sulfuric assay (53). The fractions of interest were freeze-dried and analyzed by ^{1}H and ^{31}P NMR (ENS Lyon) to confirm the PSII purification. Purified NMR-confirmed PSII was then conjugated to bovine serum albumin (BSA). The coupling reaction proceeded according to the protocol described by Romano (54), with cyanoborohydride ($NaBH_3CN$) as a coupling agent. The resulting glycoconjugate antigen (PSII-BSA) was submitted to Covalab (France) for rabbit immunization (four injections with 50 µg of the glycoconjugate per animal). Specificity of the purified PSII was confirmed by dot blot and NMR-confirmed, peptidoglycan (PG), and PG-PSII extracts.

SlpA was purified as described by Bruxelle *et al.* (55) and was submitted to Covalab (France) for guinea pig immunization (four injections with 22.5 µg of the protein per animal). Specificity of the polyclonal antibodies was performed by western blot.

Immunodetection

For the Western blot analyses, the following antibodies were used: anti-SlpA antibodies (guinea pig) diluted at 1:5,000 and anti-Cwp66 antibodies (rabbit) diluted at 1:10,000. For the dot blot analysis, anti-PSII antibodies (rabbit) diluted 1:10,000 were used. Antibody binding was revealed with anti-rabbit Immobilon Western Chemiluminescent HRP Substrate (Merck) and revelation was performed on Fusion Fx Imaging System (Vilber Lourmat).

PSII visualization by Super-Resolution Confocal microscope

A 16 h culture was diluted to obtain 10^8 cells.mL^{-1} thanks to a Kovaslide system, and 20 µL of this diluted culture was deposited on a thin round coverslip. After drying, the slides were stained in TBS-tween BSA 5%, washed, and incubated with the primary antibody (anti-PSII, 1:200) for 1h, with the secondary antibody (StarRED® from Abberior, 1:500) for 1h, and finally with Hoechst (1:2000) to visualize DNA. Washings were performed between each step. Finally, the coverslip was mounted on a slide with mounting medium Abberior Mount Solid® and stored overnight at 4°C before imaging on a STEDYCON super-resolution microscope (Abberior).

PG cytoplasmic precursors extraction and analysis

The protocol described previously by Cremniter *et al.* (56) was used with some modifications. Bacteria were grown in 500 mL brain heart infusion broth overnight and submitted to ice-cold formic acid (47mL, 1.1M) extraction for 30 min at 4 °C, without prior bacitracin treatment.

To allow comparison of the different strains whose culture optical density was not equal, we calculated the ratio peak area/optical density, presented in the results. The extract was centrifuged (7,000 x *g* for 15 min at 4 °C) and the supernatant was loaded to a gel filtration column (Sephadex G-25) for desalting. The fraction of elution was lyophilized and resuspended in 10 mL water. 100 µL of this cytoplasmic precursor solution was loaded onto an *rp*HPLC in a C18 column (Hypersil GOLD aQ; 250 x 4.6 mm; 3 µm, Thermo Scientific) at a flow rate of 1 ml/min. A linear gradient (0 to 20 %) was applied between 13 and 33 min at 25 °C (buffer A, 50 mM ammonium formate pH 4.4; buffer B, 100 % Methanol). Absorbance was monitored at 262 nm and the peak corresponding to the major cytoplasmic precursor was collected, lyophilized, resuspended in 20 µL of water. Ten µL were analyzed by mass spectrometry on a Bruker Daltonics maXis high-resolution mass spectrometer (Bremen, Germany) operating in the positive mode (Analytical platform of the Muséum National d'Histoire Naturelle, Paris, France). Mass spectral data were explored using Bruker Compass DataAnalysis 4.3.

Statistics

Statistical analyses were conducted using GraphPad Prism (version 9.0.0, GraphPad Software, San Diego, California USA, www.graphpad.com). The *p-value* is indicated for all comparisons when differences are statistically significant.

Acknowledgments

We thank Johann Peltier for providing the pMSR plasmid for allelic exchange in *C. difficile*, R.P. Fagan for the gift of pRPF185, Afi Akofa Diane Sapa for the purification of SlpA, Assilina Parfut, Marie-Emeline Zielinski and Mathieu Rodriguez for plasmids constructions. We also thank Valerie Nicolas of the platform MIPSIT of Paris Saclay University for immunofluorescence imaging. Finally, we want to thank Frederic Eghiaian from Abberior company for his help for super-resolution microscopy experiments.

Footnotes

This paper contains supplementary materials.

Funding

This work was funded by a PhD grant of the Ministère de l'Education Nationale, de l'Enseignement Supérieur, de la Recherche et de l'Innovation (MESRI) to Jeanne Malet-Villemagne and a National Institute of Allergy and Infectious Diseases (R56AI045626) grant to Yucheng Liang.

References

1. Neuhaus FC, Baddiley J. 2003. A continuum of anionic charge: structures and functions of D-alanyl-teichoic acids in gram-positive bacteria. Microbiol Mol Biol Rev 67:686–723.

2. Mesnage S, Fontaine T, Mignot T, Delepierre M, Mock M, Fouet A. 2000. Bacterial SLH domain proteins are non-covalently anchored to the cell surface via a conserved mechanism involving wall polysaccharide pyruvylation. EMBO J 19:4473–4484.

3. Willing SE, Candela T, Shaw HA, Seager Z, Mesnage S, Fagan RP, Fairweather NF. 2015. *Clostridium difficile* surface proteins are anchored to the cell wall using CWB2 motifs that recognise the anionic polymer PSII. Mol Microbiol 96:596–608.

4. Swoboda JG, Campbell J, Meredith TC, Walker S. 2010. Wall Teichoic Acid Function, Biosynthesis, and Inhibition. ChemBioChem 11:35–45.

5. Weidenmaier C, Peschel A, Xiong Y-Q, Kristian SA, Dietz K, Yeaman MR, Bayer AS. 2005. Lack of wall teichoic acids in *Staphylococcus aureus* leads to reduced interactions with endothelial cells and to attenuated virulence in a rabbit model of endocarditis. J Infect Dis 191:1771–1777.

6. Weidenmaier C, Peschel A, Kempf VAJ, Lucindo N, Yeaman MR, Bayer AS. 2005. DltABCD- and MprF-mediated cell envelope modifications of *Staphylococcus aureus* confer resistance to platelet microbicidal proteins and contribute to virulence in a rabbit endocarditis model. Infect Immun 73:8033–8038.

7. Collins LV, Kristian SA, Weidenmaier C, Faigle M, Van Kessel KPM, Van Strijp JAG, Götz F, Neumeister B, Peschel A. 2002. *Staphylococcus aureus* strains lacking D-alanine modifications of teichoic acids are highly susceptible to human neutrophil killing and are virulence attenuated in mice. J Infect Dis 186:214–219.

8. Fisher N, Shetron-Rama L, Herring-Palmer A, Heffernan B, Bergman N, Hanna P. 2006. The dltABCD operon of *Bacillus anthracis* sterne is required for virulence and resistance to peptide, enzymatic, and cellular mediators of innate immunity. J Bacteriol 188:1301–1309.

9. Spears PA, Havell EA, Hamrick TS, Goforth JB, Levine AL, Abraham ST, Heiss C, Azadi P, Orndorff PE. 2016. *Listeria monocytogenes* wall teichoic acid decoration in virulence and cell-to-cell spread. Mol Microbiol 101:714–730.

10. Meireles D, Pombinho R, Carvalho F, Sousa S, Cabanes D. 2020. *Listeria monocytogenes* Wall Teichoic Acid Glycosylation Promotes Surface Anchoring of Virulence Factors, Resistance to Antimicrobial Peptides, and Decreased Susceptibility to Antibiotics. Pathogens 9:E290.

11. Kharat AS, Denapaite D, Gehre F, Brückner R, Vollmer W, Hakenbeck R, Tomasz A. 2008. Different pathways of choline metabolism in two choline-independent strains of *Streptococcus pneumoniae* and their impact on virulence. J Bacteriol 190:5907–5914.

12. Lee SH, Wang H, Labroli M, Koseoglu S, Zuck P, Mayhood T, Gill C, Mann P, Sher X, Ha S, Yang S-W, Mandal M, Yang C, Liang L, Tan Z, Tawa P, Hou Y, Kuvelkar R, DeVito K, Wen X, Xiao J, Batchlett M, Balibar CJ, Liu J, Xiao J, Murgolo N, Garlisi CG, Sheth PR, Flattery A, Su J, Tan C, Roemer T. 2016. TarO-specific inhibitors of wall teichoic acid biosynthesis restore β-lactam efficacy against methicillin-resistant staphylococci. Science Translational Medicine 8:329ra32-329ra32.

13. Sewell EW, Brown ED. 2014. Taking aim at wall teichoic acid synthesis: new biology and new leads for antibiotics. 1. J Antibiot 67:43–51.

14. Hübscher J, Lüthy L, Berger-Bächi B, Stutzmann Meier P. 2008. Phylogenetic distribution and membrane topology of the LytR-CpsA-Psr protein family. BMC Genomics 9:617.

15. Atilano ML, Pereira PM, Yates J, Reed P, Veiga H, Pinho MG, Filipe SR. 2010. Teichoic acids are temporal and spatial regulators of peptidoglycan cross-linking in *Staphylococcus aureus*. Proc Natl Acad Sci U S A 107:18991–18996.

16. Schlag M, Biswas R, Krismer B, Kohler T, Zoll S, Yu W, Schwarz H, Peschel A, Götz F. 2010. Role of staphylococcal wall teichoic acid in targeting the major autolysin Atl. Mol Microbiol 75:864–873.

17. Bhavsar AP, Truant R, Brown ED. 2005. The TagB protein in *Bacillus subtilis* 168 is an intracellular peripheral membrane protein that can incorporate glycerol phosphate onto a membrane-bound acceptor in vitro. J Biol Chem 280:36691–36700.

18. Andre G, Deghorain M, Bron PA, van Swam II, Kleerebezem M, Hols P, Dufrene YF. 2011. Fluorescence and atomic force microscopy imaging of wall teichoic acids in *Lactobacillus plantarum*. ACS Chem Biol 6:366–376.

19. Rausch M, Deisinger JP, Ulm H, Müller A, Li W, Hardt P, Wang X, Li X, Sylvester M, Engeser M, Vollmer W, Müller CE, Sahl HG, Lee JC, Schneider T. 2019. Coordination of capsule assembly and cell wall biosynthesis in *Staphylococcus aureus*. Nat Commun 10:1404.

20. Gale RT, Li FKK, Sun T, Strynadka NCJ, Brown ED. 2017. *B. subtilis* LytR-CpsA-Psr Enzymes Transfer Wall Teichoic Acids from Authentic Lipid-Linked Substrates to Mature Peptidoglycan In Vitro. Cell Chem Biol 24:1537-1546.e4.

21. Malm S, Maaß S, Schaible UE, Ehlers S, Niemann S. 2018. In vivo virulence of *Mycobacterium tuberculosis* depends on a single homologue of the LytR-CpsA-Psr proteins. Sci Rep 8:3936.

22. Kawai Y, Marles-Wright J, Cleverley RM, Emmins R, Ishikawa S, Kuwano M, Heinz N, Bui NK, Hoyland CN, Ogasawara N, Lewis RJ, Vollmer W, Daniel RA, Errington J. 2011. A widespread family of bacterial cell wall assembly proteins. EMBO J 30:4931–4941.

23. Chan YGY, Frankel MB, Dengler V, Schneewind O, Missiakas D. 2013. *Staphylococcus aureus* mutants lacking the LytR-CpsA-Psr family of enzymes release cell wall teichoic acids into the extracellular medium. J Bacteriol 195:4650–4659.

24. Chan YG-Y, Kim HK, Schneewind O, Missiakas D. 2014. The capsular polysaccharide of *Staphylococcus aureus* is attached to peptidoglycan by the LytR-CpsA-Psr (LCP) family of enzymes. J Biol Chem 289:15680–15690.

25. Yother J. 2011. Capsules of *Streptococcus pneumoniae* and other bacteria: paradigms for polysaccharide biosynthesis and regulation. Annu Rev Microbiol 65:563–581.

26. Eberhardt A, Hoyland CN, Vollmer D, Bisle S, Cleverley RM, Johnsborg O, Håvarstein LS, Lewis RJ, Vollmer W. 2012. Attachment of capsular polysaccharide to the cell wall in *Streptococcus pneumoniae*. Microb Drug Resist 18:240–255.

27. Chu M, Mallozzi MJG, Roxas BP, Bertolo L, Monteiro MA, Agellon A, Viswanathan VK, Vedantam G. 2016. A *Clostridium difficile* Cell Wall Glycopolymer Locus Influences Bacterial Shape, Polysaccharide Production and Virulence. PLoS Pathog 12:e1005946.

28. Bartlett JG, Taylor NS, Chang T, Dzink J. 1980. Clinical and laboratory observations in *Clostridium difficile* colitis. Am J Clin Nutr 33:2521–2526.

29. Zilberberg MD, Shorr AF, Kollef MH. 2008. Increase in adult *Clostridium difficile*-related hospitalizations and case-fatality rate, United States, 2000-2005. Emerg Infect Dis 14:929–931.

30. Centers for Disease Control and Prevention (U.S.). 2019. Antibiotic resistance threats in the United States, 2019. Centers for Disease Control and Prevention (U.S.).

31. Pu M, Cho JM, Cunningham SA, Behera GK, Becker S, Amjad T, Greenwood-Quaintance KE, Mendes-Soares H, Jones-Hall Y, Jeraldo PR, Chen J, Dunny G, Patel R, Kashyap PC. 2021. Plasmid Acquisition Alters Vancomycin Susceptibility in *Clostridioides difficile*. Gastroenterology 160:941-945.e8.

32. Boekhoud IM, Hornung BVH, Sevilla E, Harmanus C, Bos-Sanders IMJG, Terveer EM, Bolea R, Corver J, Kuijper EJ, Smits WK. 2020. Plasmid-mediated metronidazole resistance in *Clostridioides difficile*. Nat Commun 11:598.

33. Ganeshapillai J, Vinogradov E, Rousseau J, Weese JS, Monteiro MA. 2008. *Clostridium difficile* cell-surface polysaccharides composed of pentaglycosyl and hexaglycosyl phosphate repeating units. Carbohydr Res 343:703–710.

34. Reid CW, Vinogradov E, Li J, Jarrell HC, Logan SM, Brisson J-R. 2012. Structural characterization of surface glycans from *Clostridium difficile*. Carbohydr Res 354:65–73.

35. Dembek M, Barquist L, Boinett CJ, Cain AK, Mayho M, Lawley TD, Fairweather NF, Fagan RP. 2015. High-throughput analysis of gene essentiality and sporulation in *Clostridium difficile*. MBio 6:e02383.

36. Peltier J, Hamiot A, Garneau JR, Boudry P, Maikova A, Hajnsdorf E, Fortier L-C, Dupuy B, Soutourina O. 2020. Type I toxin-antitoxin systems contribute to the maintenance of mobile genetic elements in *Clostridioides difficile*. Commun Biol 3:718.

628 37. Hussain HA, Roberts AP, Mullany P. 2005. Generation of an erythromycin-sensitive derivative of
629 *Clostridium difficile* strain 630 (630Deltaerm) and demonstration that the conjugative transposon
630 Tn916DeltaE enters the genome of this strain at multiple sites. J Med Microbiol 54:137–141.

631 38. Ammam F, Patin D, Coullon H, Blanot D, Lambert T, Mengin-Lecreulx D, Candela T. 2020. AsnB is
632 responsible for peptidoglycan precursor amidation in *Clostridium difficile* in the presence of
633 vancomycin. Microbiology (Reading) 166:567–578.

634 39. Liszewski Zilla M, Chan YGY, Lunderberg JM, Schneewind O, Missiakas D. 2015. LytR-CpsA-Psr
635 enzymes as determinants of *Bacillus anthracis* secondary cell wall polysaccharide assembly. J
636 Bacteriol 197:343–353.

637 40. Schaefer K, Matano LM, Qiao Y, Kahne D, Walker S. 2017. In vitro reconstitution demonstrates the
638 cell wall ligase activity of LCP proteins. Nat Chem Biol 13:396–401.

639 41. ChapetónMontes D, Candela T, Collignon A, Janoir C. 2011. Localization of the *Clostridium difficile*
640 cysteine protease Cwp84 and insights into its maturation process. J Bacteriol 193:5314–5321.

641 42. Hashizume H, Sawa R, Harada S, Igarashi M, Adachi H, Nishimura Y, Nomoto A. 2011. Tripropeptin C
642 Blocks the Lipid Cycle of Cell Wall Biosynthesis by Complex Formation with Undecaprenyl
643 Pyrophosphate. Antimicrobial Agents and Chemotherapy 55:3821–3828.

644 43. D'Elia MA, Millar KE, Beveridge TJ, Brown ED. 2006. Wall teichoic acid polymers are dispensable for
645 cell viability in *Bacillus subtilis*. J Bacteriol 188:8313–8316.

646 44. Harrison J, Lloyd G, Joe M, Lowary TL, Reynolds E, Walters-Morgan H, Bhatt A, Lovering A, Besra GS,
647 Alderwick LJ. 2016. Lcp1 Is a Phosphotransferase Responsible for Ligating Arabinogalactan to
648 Peptidoglycan in *Mycobacterium tuberculosis*. mBio 7:e00972-16.

649 45. Ballister ER, Samanovic MI, Darwin KH. 2019. *Mycobacterium tuberculosis* Rv2700 Contributes to
650 Cell Envelope Integrity and Virulence. J Bacteriol 201:e00228-19.

651 46. Sebaihia M, Wren BW, Mullany P, Fairweather NF, Minton N, Stabler R, Thomson NR, Roberts AP,
652 Cerdeño-Tárraga AM, Wang H, Holden MTG, Wright A, Churcher C, Quail MA, Baker S, Bason N,
653 Brooks K, Chillingworth T, Cronin A, Davis P, Dowd L, Fraser A, Feltwell T, Hance Z, Holroyd S, Jagels
654 K, Moule S, Mungall K, Price C, Rabbinowitsch E, Sharp S, Simmonds M, Stevens K, Unwin L,
655 Whithead S, Dupuy B, Dougan G, Barrell B, Parkhill J. 2006. The multidrug-resistant human
656 pathogen *Clostridium difficile* has a highly mobile, mosaic genome. Nat Genet 38:779–786.

657 47. Gibson DG, Glass JI, Lartigue C, Noskov VN, Chuang R-Y, Algire MA, Benders GA, Montague MG, Ma
658 L, Moodie MM, Merryman C, Vashee S, Krishnakumar R, Assad-Garcia N, Andrews-Pfannkoch C,
659 Denisova EA, Young L, Qi Z-Q, Segall-Shapiro TH, Calvey CH, Parmar PP, Hutchison CA, Smith HO,
660 Venter JC. 2010. Creation of a bacterial cell controlled by a chemically synthesized genome. Science
661 329:52–56.

662 48. Pryor JM, Potapov V, Kucera RB, Bilotti K, Cantor EJ, Lohman GJS. 2020. Enabling one-pot Golden
663 Gate assemblies of unprecedented complexity using data-optimized assembly design. PLoS One
664 15:e0238592.

665 49. Pryor JM, Potapov V, Bilotti K, Pokhrel N, Lohman GJS. 2022. Rapid 40 kb Genome Construction
666 from 52 Parts through Data-optimized Assembly Design. ACS Synth Biol 11:2036–2042.

667 50. Cartman ST, Kelly ML, Heeg D, Heap JT, Minton NP. 2012. Precise manipulation of the *Clostridium*
668 *difficile* chromosome reveals a lack of association between the tcdC genotype and toxin
669 production. Appl Environ Microbiol 78:4683–4690.

670 51. Fagan R, Fairweather N. 2010. Dissecting the cell surface. Methods Mol Biol 646:117–134.

671 52. Cox AD, St Michael F, Aubry A, Cairns CM, Strong PCR, Hayes AC, Logan SM. 2013. Investigating the
672 candidacy of a lipoteichoic acid-based glycoconjugate as a vaccine to combat *Clostridium difficile*
673 infection. Glycoconj J 30:843–855.

674 53. DuBois Michel, Gilles KA, Hamilton JK, Rebers PA, Smith Fred. 1956. Colorimetric Method for
675 Determination of Sugars and Related Substances. Anal Chem 28:350–356.

676 54. Romano MR, Leuzzi R, Cappelletti E, Tontini M, Nilo A, Proietti D, Berti F, Costantino P, Adamo R,
677 Scarselli M. 2014. Recombinant *Clostridium difficile* toxin fragments as carrier protein for PSII
678 surface polysaccharide preserve their neutralizing activity. Toxins (Basel) 6:1385–1396.

679 55. Bruxelle J-F, Mizrahi A, Hoys S, Collignon A, Janoir C, Péchiné S. 2016. Immunogenic properties of
680 the surface layer precursor of *Clostridium difficile* and vaccination assays in animal models.
681 Anaerobe 37:78–84.

682 56. Cremniter J, Mainardi J-L, Josseaume N, Quincampoix J-C, Dubost L, Hugonnet J-E, Marie A,
683 Gutmann L, Rice LB, Arthur M. 2006. Novel mechanism of resistance to glycopeptide antibiotics in
684 *Enterococcus faecium*. J Biol Chem 281:32254–32262.

685 57. Trieu-Cuot P, Carlier C, Poyart-Salmeron C, Courvalin P. 1990. A pair of mobilizable shuttle vectors
686 conferring resistance to spectinomycin for molecular cloning in *Escherichia coli* and in Gram-
687 positive bacteria. Nucleic Acids Research 18:4296.

688 58. Fagan RP, Fairweather NF. 2011. *Clostridium difficile* Has Two Parallel and Essential Sec Secretion
689 Systems. J Biol Chem 286:27483–27493.

690 59. Heap JT, Pennington OJ, Cartman ST, Minton NP. 2009. A modular system for *Clostridium* shuttle
691 plasmids. J Microbiol Methods 78:79–85.

Figures legends

Figure 1

The Δ*lcpB* mutant (JMV4) presents curved, inflated, longer and larger cells than the parental strain JMV1.

A. JMV3 (**Δ*lcpA*)** and JMV4 (**Δ*lcpB)*** single mutants were analyzed in optic microscopy and complemented with pMTL84222 (vector), p*lcpA* (plasmid carrying *lcpA* expressed with its own promoter) or p*lcpB* (plasmid carrying *lcpB* expressed with its own promoter). Scale bar represents 20µm. **B.** The percentage of abnormal (curved, thick, or inflated) cells among total cells was calculated by measuring more than 100 cells for each strain. **C.** Cell length of the parental strain JMV1, JMV3 and JMV4 complemented with the vector (pMTL84222), p*lcpA* or p*lcpB*. **D.** Cell width of the parental strain JMV1, JMV3 and JMV4 complemented with the vector (pMTL84222), p*lcpA* or p*lcpB*. For B, C and D, the number above each group data represents the number of cells counted. **** means student t-test *p-value* is< 0.0001.

Figure 2

Both *lcpA* and *lcpB* have a constitutive expression

GusA activity measured for *lcpA* (**A**) and *lcpB* (**B**) promoters GusA activity (blue curve) was measured in Miller Units and growth (red curve) was followed by measuring the optical density at 600 nm (OD_{600nm}) for 8 hours.

Figure 3

Both Δ*lcpA* and Δ*lcpB* exhibit an altered PSII layer at the surface.

Immunofluorescence assay of JMV1, JMV3 and JMV4 strains, was observed using super-resolution microscope. Bacteria were stained for DNA (DAPI, blue) and PSII (anti-PSII, green). The merged picture shows both localizations simultaneously (scale bar represents 20 µm). The panel shows a magnify part of the picture (scale bar represents 2 µm).

Figure 4

The *lcp* conditional-lethal mutant (JMV6) is not able to grow without ATc induction of the P_{tet}-*lcpB* copy.

A. JMV1 and JMV2 grown in liquid culture were diluted and plated on BHI agar petri dishes. JMV6 grown in liquid culture in the presence of 10 (JMV6 (ATC 10)) or 50 ng.mL^{-1} (JMV6 (ATc 50)) of ATc was diluted and plated on BHI agar petri dishes. The control strain, JMV6 harboring the plasmid p*lcpA* grown in liquid culture in the presence of 50 ng.mL^{-1} of ATc (JMV6 + p*lcpA* (ATc 50)) was diluted and plated on BHI agar petri dishes. Petri dishes contained ATc from 0 to 250 ng.mL^{-1} in the BHI agar medium. **B.** JMV1, JMV2, JMV6 and JMV6 + p*lcpA* were grown in the presence of 50 ng.mL^{-1} of ATc and then, the growth was measured for 20h (1200 minutes) without ATc (JMV1, JMV6 + p*lcpA*), in the presence of 10 ng.mL^{-1} of ATc (JMV6 (ATc 10)) or in the presence of 50 ng.mL^{-1} of ATc (JMV2 (ATc 50), JMV6 (ATc 50), JMV6 + p*lcpA* (ATc 50)). The graph represents the mean of 3 independent experiments.

Figure 5

738 **In the presence of 10 ng.mL^{-1} of ATc, the *lcp* conditional-lethal mutant (JMV6)**
739 **loses its rod shape.**
740 **A**. JMV1, JMV6 + p*lcpA*, JMV6 + p*lcpB*, JMV2 in the presence of 50 ng.mL^{-1} (JMV2
741 (ATc 50)) of ATc and JMV6 in the presence of 10 (JMV6 (ATc 10)) or 50 ng.mL^{-1} (JMV6
742 (ATc 50) of ATc were observed in optic microscopy. The scale bar represents 20 µm.
743 **B** and **C**. Cell length (**B**) and cell width (**C**) of bacteria from each strain observed in **A**.
744 were measured. The number above each group data represents the number of cells
745 counted. **** means student t-test *p-value* is< 0.0001.
746
747 Figure 6
748 **In the presence of 10 ng.mL^{-1}** of **ATc , the *lcp* conditional-lethal mutant (JMV6)**
749 **loses its rod shape but PSII is still detected at the surface.**
750 Immunofluorescence assay of JMV1, JMV2 in the presence of 50 ng.mL^{-1} (JMV2
751 (ATc50)), JMV6 in the presence of 10 ng.mL^{-1} (JMV6 (ATc10)), JMV6 in the presence of
752 50 ng.mL^{-1} (JMV6 (ATc50)) and JMV6 + p*lcpA* in the presence of 50 ng.mL^{-1} (JMV6 +
753 p*lcpA* (ATc50)) strains was observed using super-resolution microscope. Bacteria were
754 stained for DNA (DAPI, blue) and PSII (anti-PSII, green). The merged picture shows
755 both localizations simultaneously (scale bar represents 20µm). The panel shows a
756 magnify part of the picture (scale bar represents 2µm).
757
758 Figure 7
759 **PSII is released into the supernatant of the JMV6 strain in the presence of**
760 **10 ng.mL^{-1} of ATc**

761 Dot blot analysis using specific antibodies targeting PSII was performed on the bacterial
762 surface content (pellet) and supernatant content (culture supernatant) from JMV1, JMV2
763 JMV3, JMV4, JMV6 grown in the presence of 10 ng.mL^{-1} of Atc (JMV6 (Atc 10)), JMV6
764 grown in the presence of 50 ng.mL^{-1} of Atc (JMV6 (Atc 50)) and JMV6 p*lcpA* grown in
765 the presence of 50 ng.mL^{-1} of Atc (JMV6 + p*lcpA* (Atc 50)). Each content was diluted up
766 to 1:64. PG-PSII is used as positive control and PG as a negative control.
767
768 Figure 8
769 **PSII anchoring impairment is associated with Cwp proteins released in the culture**
770 **supernatant.**
771 Characterization of surface (**A**, **C**, **E**) and supernatant (**B**, **D**, **F**) protein profiles from
772 JMV1, JMV2, JMV6 and JMV6 + p*lcpA* grown in the absence of Atc (-) or in the
773 presence of 10 ng.mL^{-1} of Atc (10) or in the presence of 50 ng.mL^{-1} of Atc (50).
774 Coomassie blue staining (**A, B**), anti-Cwp66 Western blots (**C, D**) and anti-SlpA Western
775 blots (**E, F**) were performed. The protein ladder is graduated in kg Dalton (kDa). MW:
776 molecular weight.
777
778 Figure 9
779 **PSII anchoring mutants present an autolysis phenotype**
780 Autolysis of JMV1, JMV3 and JMV4, harboring the empty plasmid pMTL84222 (+
781 vector), the p*lcpA* plasmid (+ p*lcpA*) or the p*lcpB* plasmid (+ p*lcpB*) were measured and
782 presented in **A**. Autolysis of JMV1, JMV2 grown in the presence of 50 ng.mL^{-1} of ATc
783 (50), JMV6 + p*lcpA*, JMV6 grown in the presence of 10 ng.mL^{-1} of ATc (JMV6 (ATc10)),
784 JMV6 grown in the presence of 50 ng.mL^{-1} of ATc (JMV6 (ATc50)) and JMV6 + p*lcpA*

grown in the presence of 50 ng.mL^{-1} of ATc (JMV6 + p*lcpA* (ATc50)), were measured and presented in **B**. The optical density was measured for 3 hours (180 minutes) and the result is presented as a cell survival percentage. The graph represents the mean of 3 independent experiments.

Figure 10

PG cytoplasmic precursors accumulate when PSII anchoring is impaired

A, **B** and **C**. Purification and quantification of UDP-Mur*N*Ac-pentapeptide from JMV1 (**A**), JMV6 grown in the presence of 10 ng.mL^{-1} of ATc (JMV6 (ATc10)) (**B**), JMV6 + p*lcpA* grown in the presence of 50 ng.mL^{-1} of ATc (JMV6 + p*lcpA* (ATc50)) (**C**) was performed. **D**. A table represents each peak area and area/optical density ratio. In addition, the observed and calculated monoisotopic masses obtained after mass spectrometry analysis are presented in the two last columns. mAU = milli Arbitrary Unit, Da = Dalton

Supplemental figures legends

Figure S1

Graphic map of the pJV10 plasmid used to construct deletion plasmids of the *lcp*

On this graphic map of the pJV10 plasmid, created by Serial Cloner, the spectinomycin resistance gene flanked by BsaI sites to allow Golden Gate assembly, an erythromycin resistance gene, and the P_{tet}-CD2517 (Toxin) from the pMSR to facilitate counterselection during the allelic exchange are shown.

Figure S2

The Δ*lcpB* strain presents an altered growth

Growth curve of single mutant strains of *lcpA* (JMV3) *and lcpB* (JMV4), harboring either the pMTL84222, or the p*lcpA* or p*lcpB* plasmid. The growth was observed in BHI medium for 17 hours (1020 minutes). The graph represents the mean of 3 independent experiments.

Figure S3

The Δ*lcpB* mutant (JMV4) is thicker, curved, or inflated in liquid culture.

These panels present additional pictures of the JMV4 strain observed in optic microscopy. The scale bar represents 20 µm.

Figure S4

The single *lcp* mutants JMV3 and JMV4 exhibit a normal S-layer content

This Coomassie staining of Cwp protein extractions shows that the Cwp content of the S-layer of JMV1, JMV3 and JMV4 harboring either pMTL84222 (vector), p*lcpA* or p*lcpB* plasmid. The protein ladder is graduated in kg Dalton (kDa). MW: molecular weight.

Figure S5

The PSII was obtained and the absence of contamination with LTA was confirmed by NMR.

^{1}H (**A**) and ^{31}P (**B**) NMR spectra of the PSII extracted from culture pellets of the 630 strain. Two samples were sent for analysis, named PSII 3.2 and PSII 2.6. Both were confirmed to contain PSII. The chemical shift is measured in part-per-million (ppm).

Figure S6

The immunization led to antibodies production and these antibodies showed good specificity for the PSII

This dot blot assay shows that the antibodies produced by the rabbits recognize well the RMN-verified PSII (**A**) of *C. difficile* and the PG linked PSII (PG-PSII) (**A** and **C**) and do not cross-react with peptidoglycan (**A** and **C**) or lipoteichoic acid (LTA) (**C**) of *C. difficile*. Moreover, different samples at different stages of the purification process were tested (**B**). Briefly, PSII purification protocol was performed as followed (white boxes, steps of PSII purification, yellow boxes, potential contaminant molecules) : 1 litter of *C. difficile* culture was pelleted. Pellet was washed in PBS and boiled in water for 30 minutes. After centrifugation, pellet (a) was tested to know whether some PSII were not recovered. The supernatant was further used for purification and a TCA precipitation was performed. After centrifugation, pellet (b) was tested to know whether some PSII was not recovered; it was resuspended in water and centrifuged again, giving pellet (c). The supernatant (d) was dialyzed and applied on fPLC. PSII was recovered, dosage was performed by phenol sulfuric method and PSII was analyzed by NMR.

Figure S7

A new strategy designed to construct a conditional-lethal mutant in *C. difficile*

Schematic representation of the strategy used to create a conditional-lethal mutant of *C. difficile lcpA* and *lcpB* genes. The strategy consists in three major steps: first the insertion of an inducible copy of *lcpB* in the *erm* locus of the chromosome (under control of P_{tet}), then the deletion of both *lcpA* and *lcpB* by replacing the ORFs with a *catP* gene, and finally the control of the *I* expression of *lcpB* thanks to ATc induction.

Figure S8

The anchoring of PSII is essential for *C. difficile* growth

The conditional-lethal mutant pre-cultured overnight in liquid BHI in the presence of 50 ng.mL^{-1}ATc is not able to grow on a BHI plate without ATc but grows correctly in the presence of ATc at 50 ng.mL^{-1}.

865 Tables :

866

867 Table 1. Bacterial strains and plasmids used in this study.

Name	Genotype or primer sequence	Source or reference
Bacterial strains		
Escherichia coli		
TG1	*E. coli* k12 (F', *tra* D36, *lacIq*, Δ*lacZ*, MIS, *pro* A+B+/SupE, Δ(*hdsM-mcrB*))	Laboratory stock
HB101 pRK24	*E. coli* (pRK24) (F - Δ(*gpt-proA*) 62 Leu B6 *gln* V44 *ara*-14 *gal*K2 *lac*Y1 Δ(*mcrC-mrr*) *rps* L20 (*srt*^{r}) *xyl*-5 *mlt*-1 *rec* A13, pRK24	Laboratory stock
Clostridioides difficile		
630	Clinical strain, Erm^R	Sebaihia *et al.* 2006 (46)
630Δ*erm*	Derivative of 630 strain, Erm^S	Hussain *et al.* 2005 (37)
JMV1	Derivative of 630 strain, Erm^S, Δ(*CD630_20100*, *CD630_20091*, *CD630_20090*, *CD630_20080*, *CD630_20071*, *CD630_20070*)	This work
JMV2 (630 P_{tet}-*lcpB)*	Derivative of 630 strain, Erm^S, Δ(*CD630_20100*, *CD630_20091*, *CD630_20090*, *CD630_20080*, *CD630_20071*, *CD630_20070*)::P_{tet}-*lcpB*	This work
JMV3 (Δ*lcpA)*	JMV1 Δ*lcpA*	This work
JMV4	JMV1 Δ*lcpB*	This work
JMV5 (Δ*lcpB* P_{tet}-*lcpB)*	JMV2 Δ*lcpB*	This work
JMV6 (Δ*lcpA* Δ*lcpB* P_{tet}-*lcpB*)	JMV2 Δ*lcpA* Δ*lcpB*	This work
Plasmids and vectors		
pMSR	Circular cloning vector, 5624 nucleotides, *catP*, α*lacZ,* P_{tet}-*CD2517* (toxin), pseudo-suicide plasmid, Cm^R	Gift from J. Peltier (36)
pBLUNT	Linear cloning vector from Invitrogen, Kn^R	Invitrogen

pAT28	Mobilizable shuttle plasmid, Spc^R	Trieu-Cuot *et al.* 1990 (57)
pRPF185	P_{tet}-*gusA* $Tm^{R,}$ expression and cloning vector	Fagan *et al.* 2011 (58)
pMTL-83151	Cm^R cloning vector, pCB102 replicative origin	Heap *et al.* 2009 (59)
pMTL-84151	Cm^R cloning vector, pCD6 replicative origin	
pMTL-84222	Erm^R cloning vector, pCD6 replicative origin	
pJV4	pBLUNTΩ*aadA*, spectinomycin resistance gene flanked by BsaI sites, Kn^R	This work
pJV5	pMSR derivative, used to construct pJV8, Cm^R and Sp^R	This work
pJV6	pMTL-83151Δ*catP*Ω*ermB*, Erm^R	This work
pJV7	pMSRΩ*aadA,* spectinomycin resistance gene flanked by BsaI sites, Cm^R and Sp^R	This work
pJV8	pMSR derivative, plasmid used for Erm locus deletion, $Cm^{R,}$ and Sp^R	This work
pJV10	pJV7Δ*catP*Ω*ermB*, Erm^R and Sp^R	This work
pJV11	pJV10 derivative, plasmid used for *lcpA* deletion plasmid, Erm^R	This work
pJV12	pJV10 derivative, plasmid used for *lcpB* deletion plasmid, Erm^R	This work
pJV13	pJV10 derivative, plasmid used for *lcp* region deletion, Erm^R	This work
pTC131	pMTL-84151Ω*aadA,* spectinomycin resistance gene flanked by BsaI sites, Cm^R and Sp^R	This work
pMEZ5	pTC131Δ*catP*Ω*ermB,* Erm^R and Sp^R	This work
p*lcpA* (pMEZ12)	pMEZ-5ΩP_{lcpA}-*lcpA*, Erm^R	This work
pJV20	pTC131ΩP_{lcpB}-*lcpB*, Cm^R	This work
p*lcpB* (pJV21)	pMTL-84222ΩP_{lcpB}-*lcpB*, Erm^R	This work
pJV27	pJV8ΩP_{tet}-*lcpB*, Cm^R	This work
pMDR1	pTC131Ω*aphA*Ω*gusA*, $Cm^{R,}$ and Kn^R	This work
pMDR2	pMDR1Δ*aphA*Ω*aadA*, Cm^R and Sp^R	This work
pMDR5	pMDR2Δ*aadA*ΩP_{lcpB}, Cm^R	This work
pMDR8	pMDR2Δ*aadA*ΩP_{lcpA}, Cm^R	This work

868

869

Authors contributions

Conceptualization: TC, JMV

Funding acquisition: TC, JMV,CJ

Experimental work: JMV, TC

PSII purification and RMN: JMV, LE, SDQ

PG precursors experiment: YL, JH, MA, JMV

Supervision: TC

Writing original draft: TC, JMV

Validation: JMV, TC, LE, SDQ, YL, JH, MA, CJ

Conflicts of interest

The authors declare that they have no conflicts of interest with the contents of this article.

Abbreviations used

ATc: anhydrotetracycline

CWGPs: cell wall glycopolymers

MW: molecular weight

PSII: polysaccharide II

PG: peptidoglycan

$C_{55}P$: C_{55}-undecaprenyl phosphate

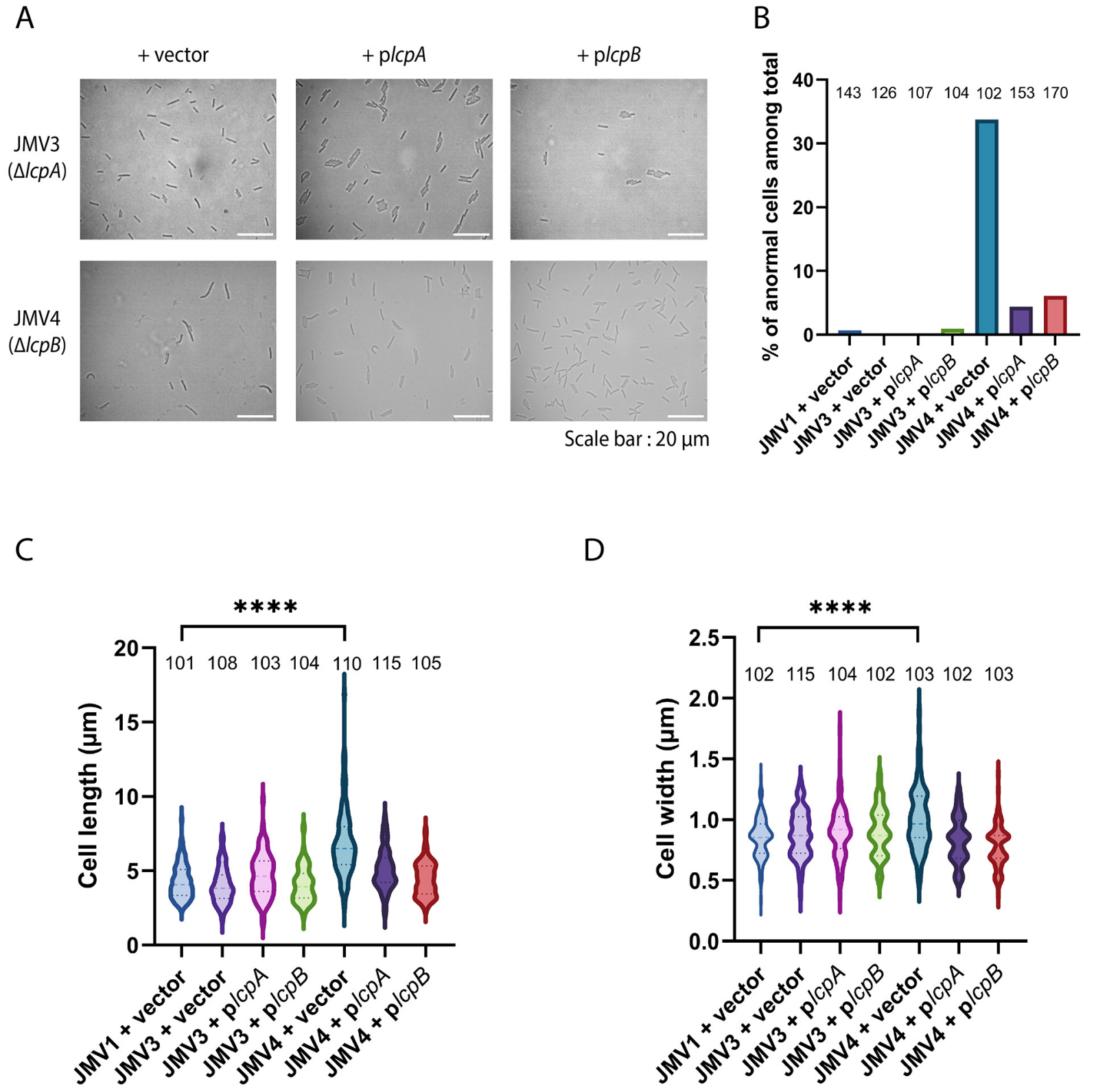
A
+ vector
+ pIcpA
+ pIcpB
JMV3 (ΔIcpA)
JMV4 (ΔIcpB)
Scale bar : 20 µm
B
% of anormal cells among total
143 126 107 104 102 153 170
JMV1 + vector
JMV3 + vector
JMV3 + pIcpA
JMV3 + pIcpB
JMV4 + vector
JMV4 + pIcpA
JMV4 + pIcpB
C
****
Cell length (µm)
101 108 103 104 110 115 105
D
****
Cell width (µm)
102 115 104 102 103 102 103

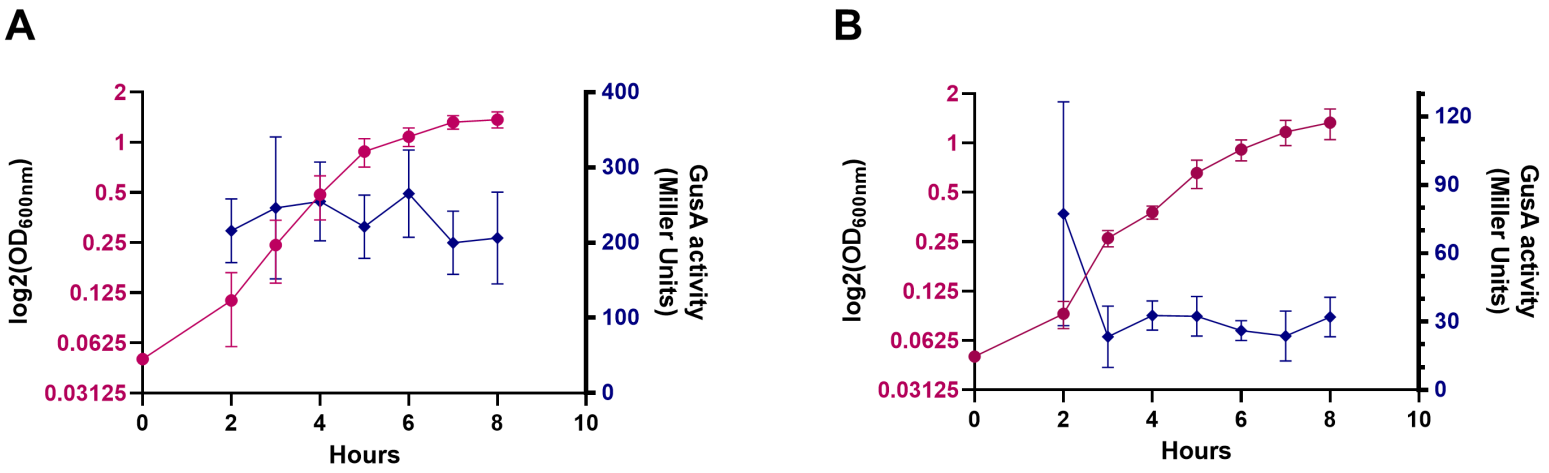
A
log2(OD600nm)
2
1
0.5
0.25
0.125
0.0625
0.03125
0
2
4
6
8
10
Hours
400
300
200
100
0
GusA activity
(Miller Units)
B
log2(OD600nm)
2
1
0.5
0.25
0.125
0.0625
0.03125
0
2
4
6
8
10
Hours
120
90
60
30
0
GusA activity
(Miller Units)

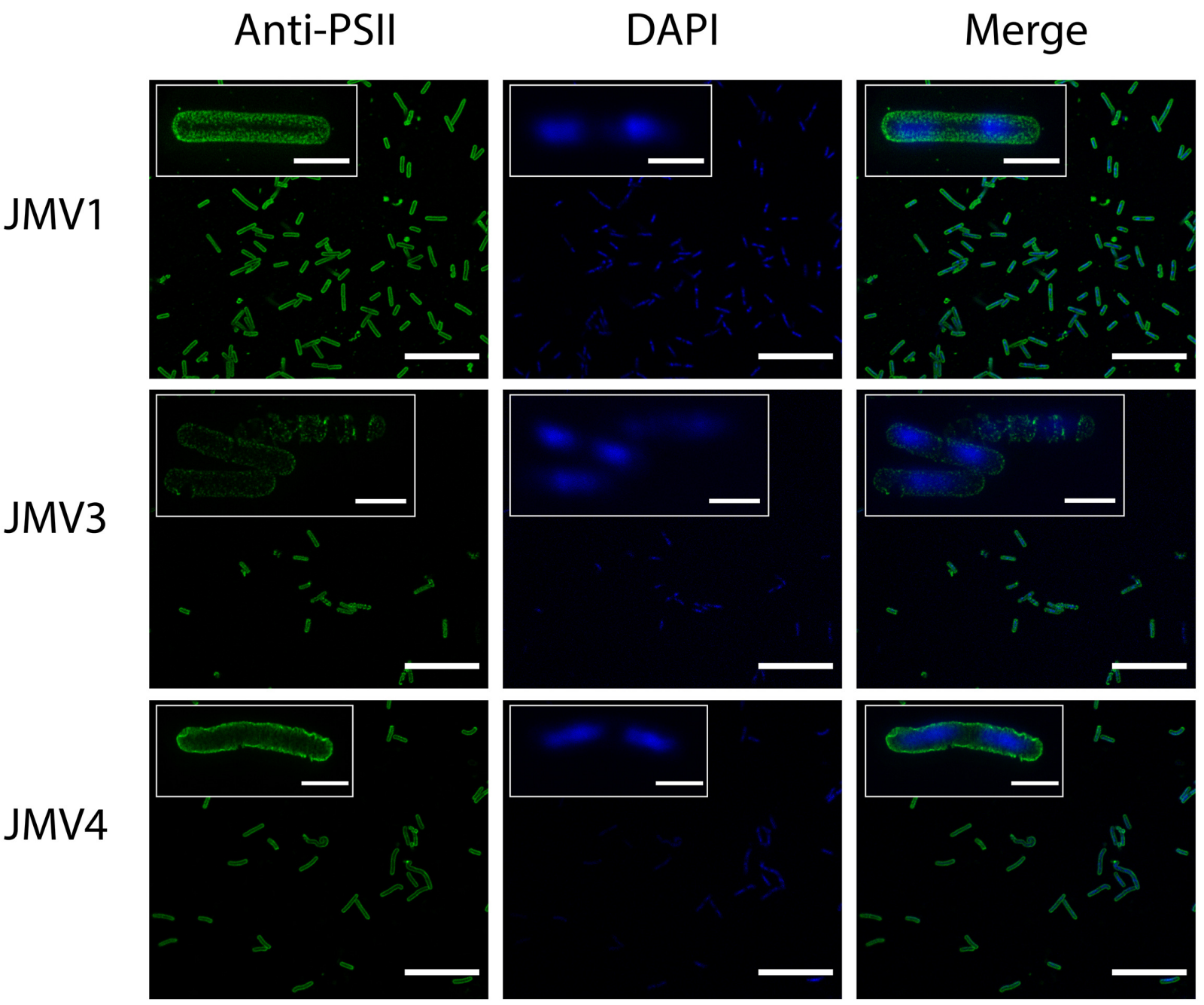
Anti-PSII
DAPI
Merge
JMV1
JMV3
JMV4
Scale bars : inserts = 2 µm large views = 20 µm

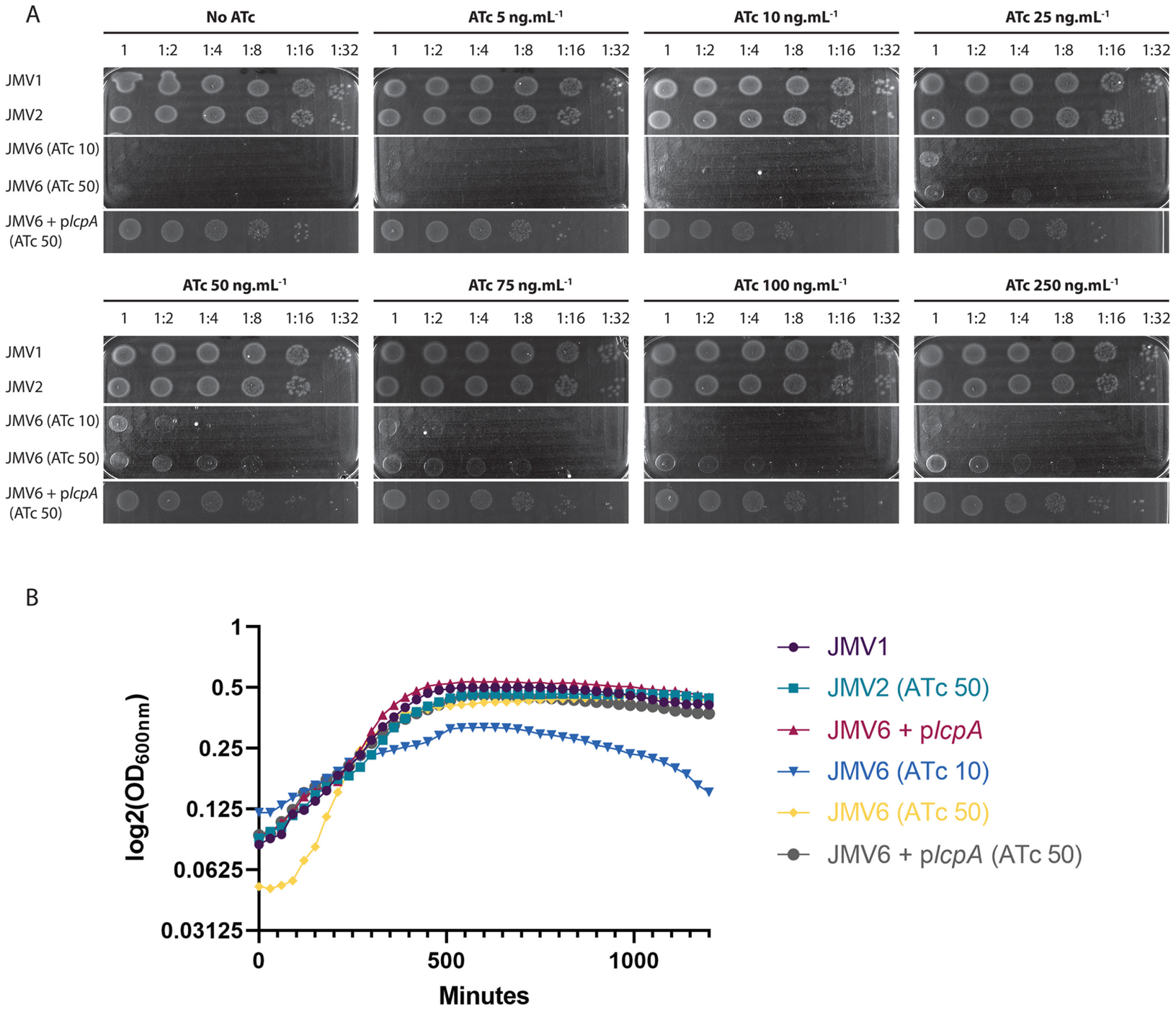
A
No ATc
ATc 5 ng.mL-1
ATc 10 ng.mL-1
ATc 25 ng.mL-1
ATc 50 ng.mL-1
ATc 75 ng.mL-1
ATc 100 ng.mL-1
ATc 250 ng.mL-1
1
1:2
1:4
1:8
1:16
1:32
JMV1
JMV2
JMV6 (ATc 10)
JMV6 (ATc 50)
JMV6 + plcpA (ATc 50)
B
log2(OD600nm)
1
0.5
0.25
0.125
0.0625
0.03125
0
500
1000
Minutes
JMV1
JMV2 (ATc 50)
JMV6 + plcpA
JMV6 (ATc 10)
JMV6 (ATc 50)
JMV6 + plcpA (ATc 50)

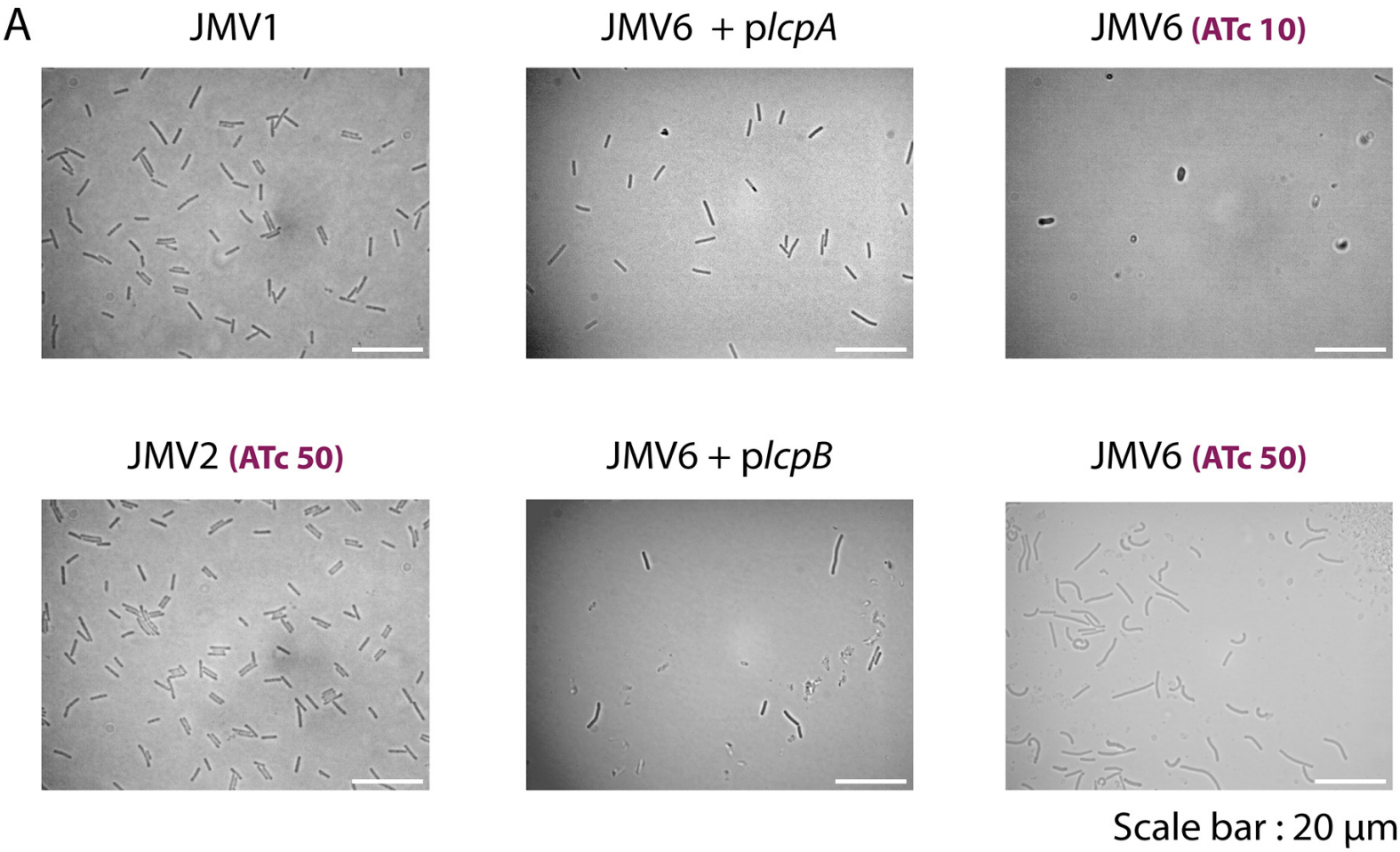
A
JMV1
JMV6 + p*lcpA*
JMV6 (ATc 10)
JMV2 (ATc 50)
JMV6 + p*lcpB*
JMV6 (ATc 50)
Scale bar : 20 µm

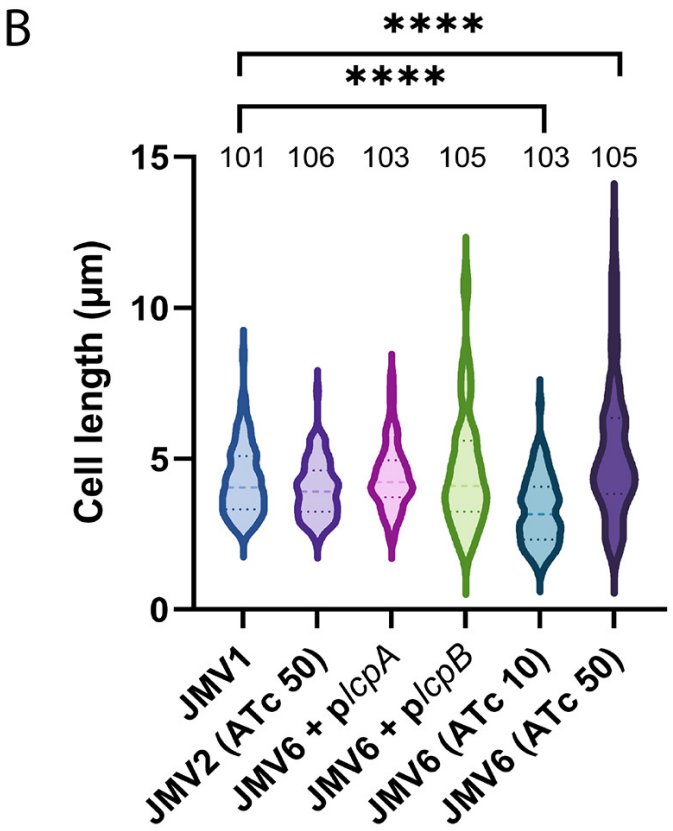
B
****
****
101 106 103 105 103 105
Cell length (µm)
15
10
5
0
JMV1
JMV2 (ATc 50)
JMV6 + p*lcpA*
JMV6 + p*lcpB*
JMV6 (ATc 10)
JMV6 (ATc 50)

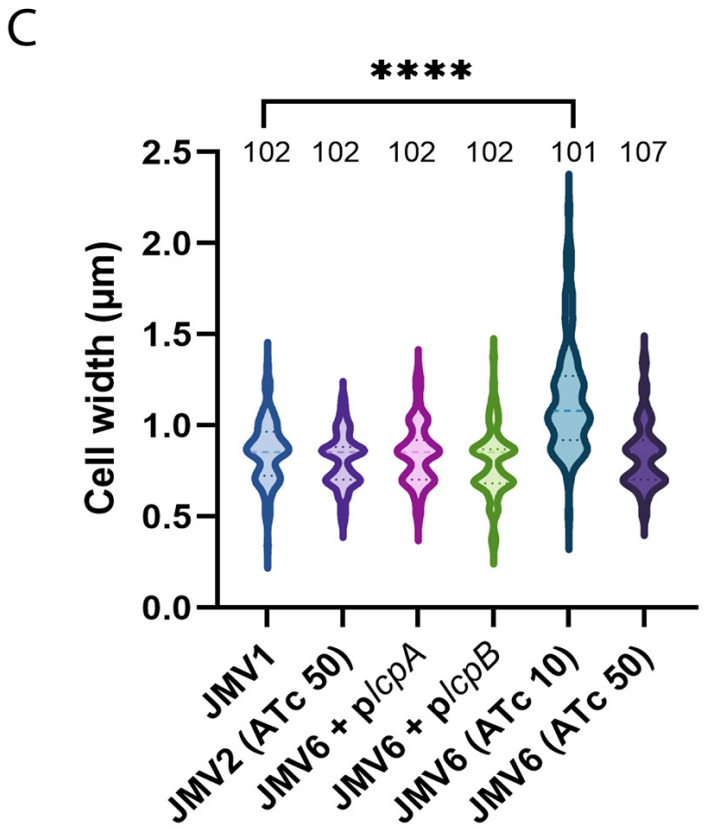
C
****
102 102 102 102 101 107
Cell width (µm)
2.5
2.0
1.5
1.0
0.5
0.0
JMV1
JMV2 (ATc 50)
JMV6 + p*lcpA*
JMV6 + p*lcpB*
JMV6 (ATc 10)
JMV6 (ATc 50)

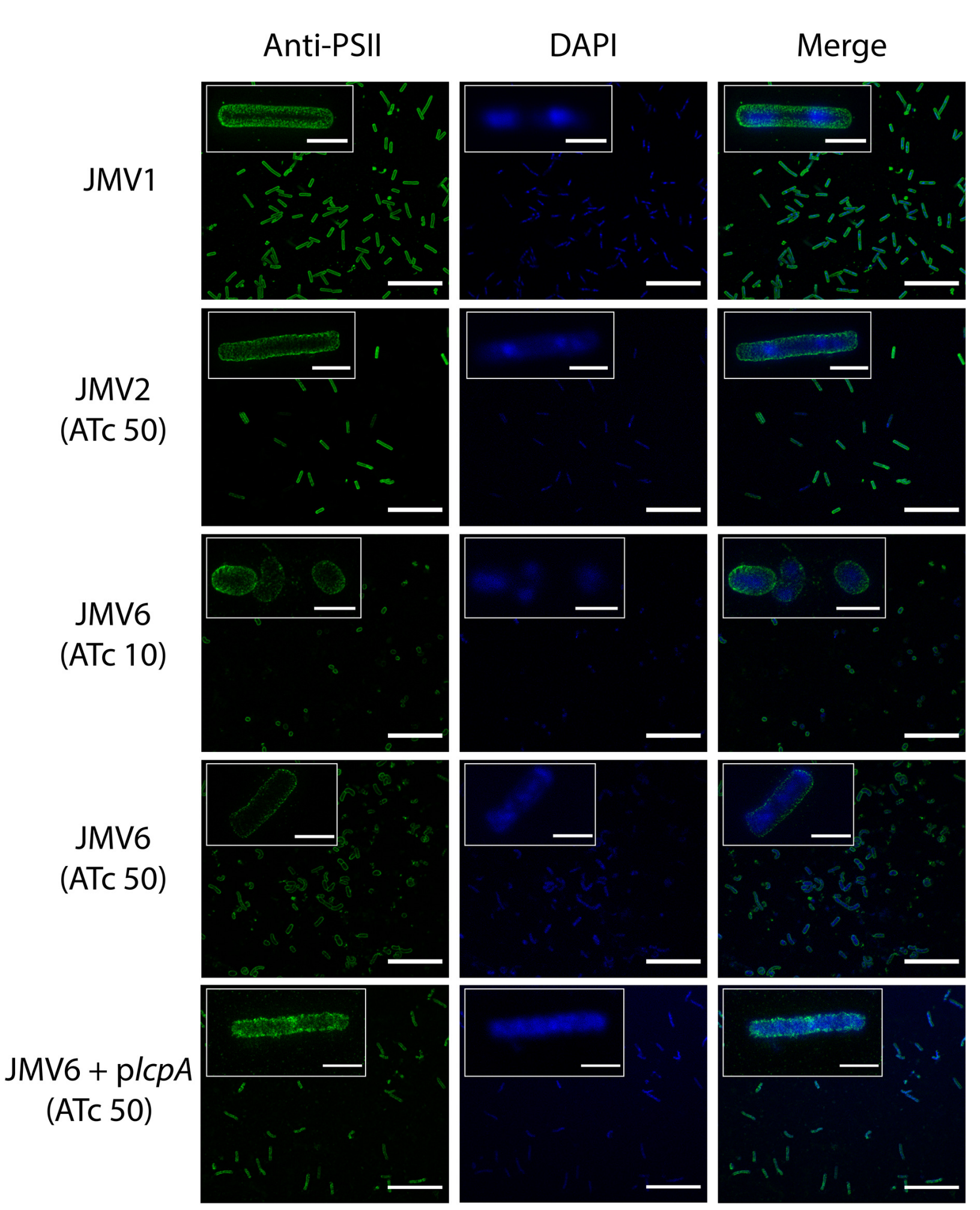
Anti-PSII
DAPI
Merge
JMV1
JMV2
(ATc 50)
JMV6
(ATc 10)
JMV6
(ATc 50)
JMV6 + p*lcpA*
(ATc 50)
Scale bars : inserts = 2 µm large views = 20 µm

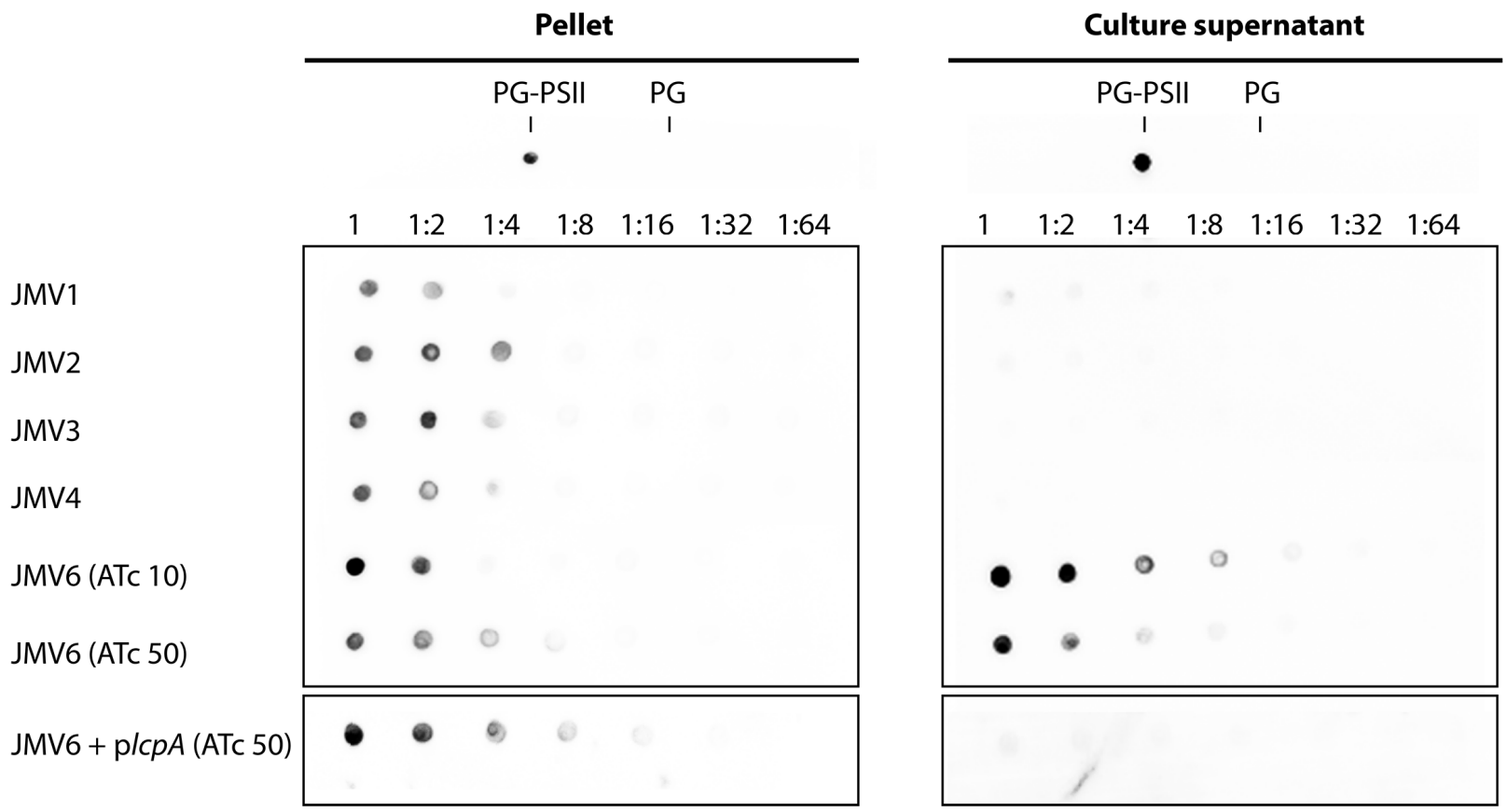
Pellet
Culture supernatant
PG-PSII
PG
PG-PSII
PG
1
1:2
1:4
1:8
1:16
1:32
1:64
1
1:2
1:4
1:8
1:16
1:32
1:64
JMV1
JMV2
JMV3
JMV4
JMV6 (ATc 10)
JMV6 (ATc 50)
JMV6 + p*lcpA* (ATc 50)

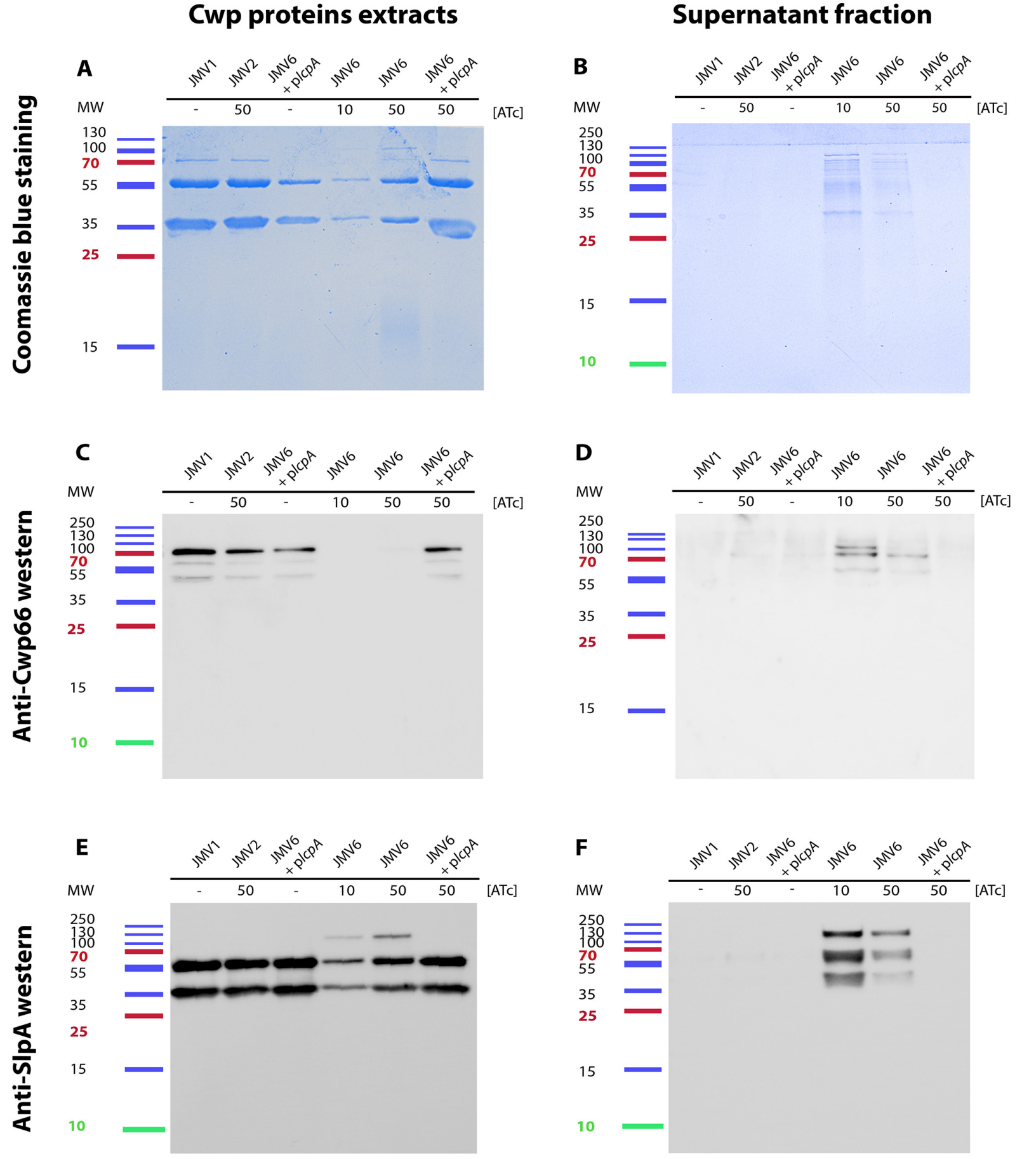
Cwp proteins extracts
Supernatant fraction
Coomassie blue staining
Anti-Cwp66 western
Anti-SlpA western
A
B
C
D
E
F
JMV1
JMV2
JMV6 + pIcpA
JMV6
JMV6
JMV6 + pIcpA
MW
-
50
-
10
50
50
[ATc]
250
130
100
70
55
35
25
15
10

A

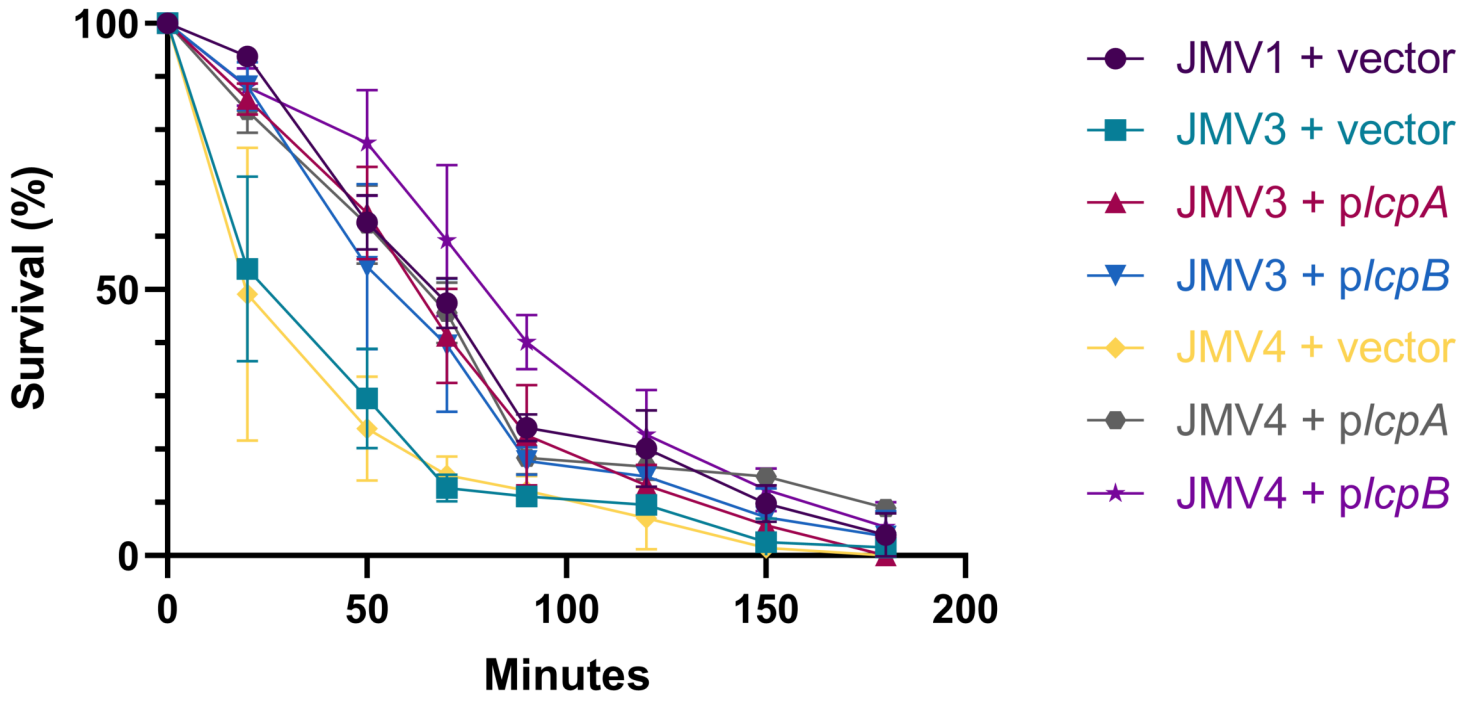
100
50
0
Survival (%)
0
50
100
150
200
Minutes
JMV1 + vector
JMV3 + vector
JMV3 + plcpA
JMV3 + plcpB
JMV4 + vector
JMV4 + plcpA
JMV4 + plcpB

B

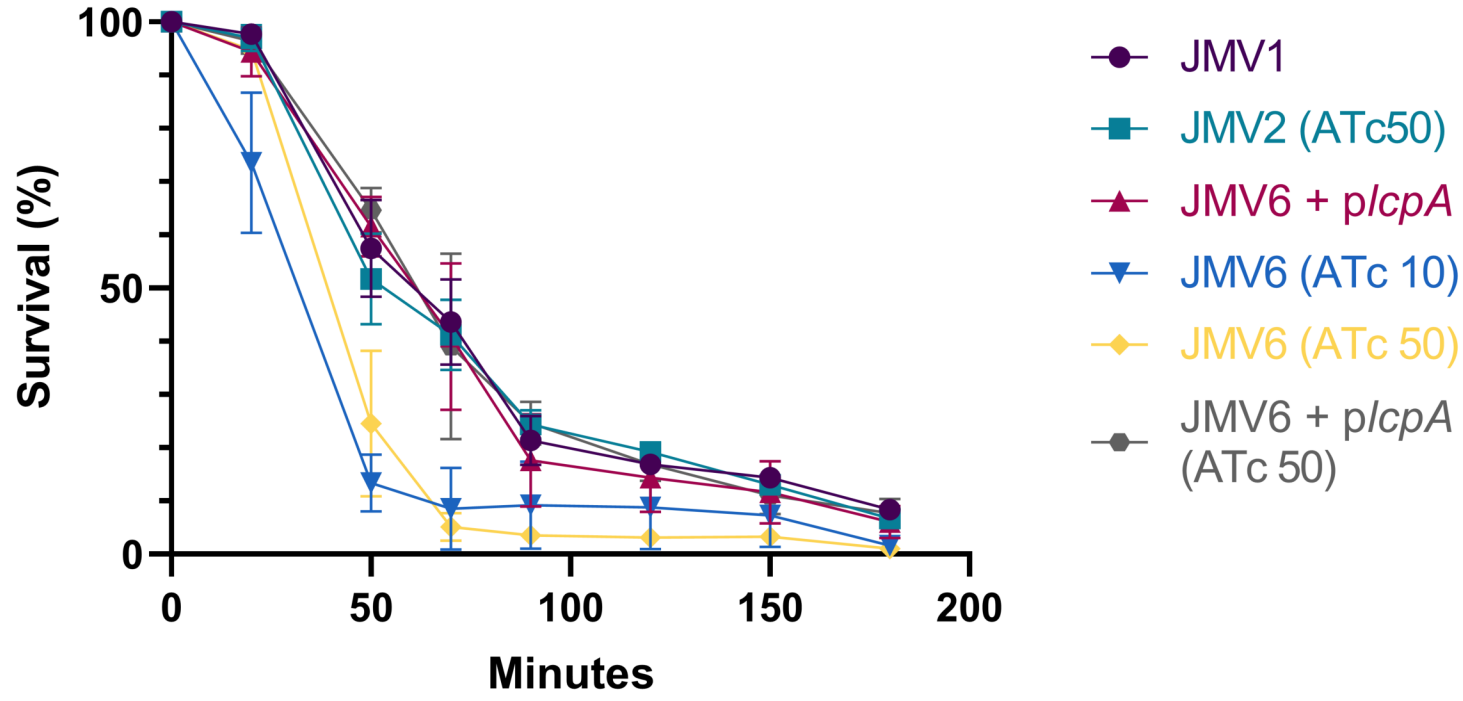
100
50
0
Survival (%)
0
50
100
150
200
Minutes
JMV1
JMV2 (ATc50)
JMV6 + plcpA
JMV6 (ATc 10)
JMV6 (ATc 50)
JMV6 + plcpA (ATc 50)

A JMV1

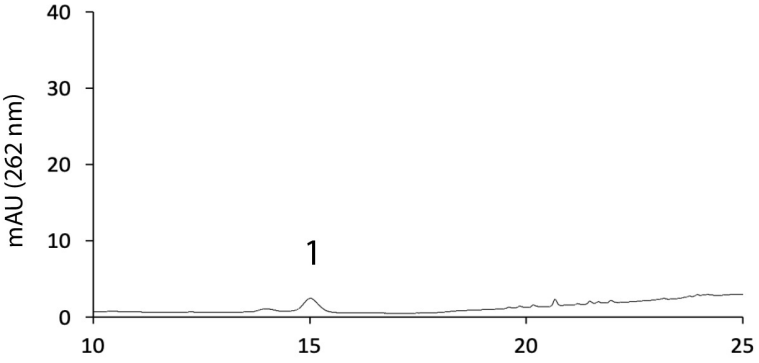

B JMV6 (ATc 10)

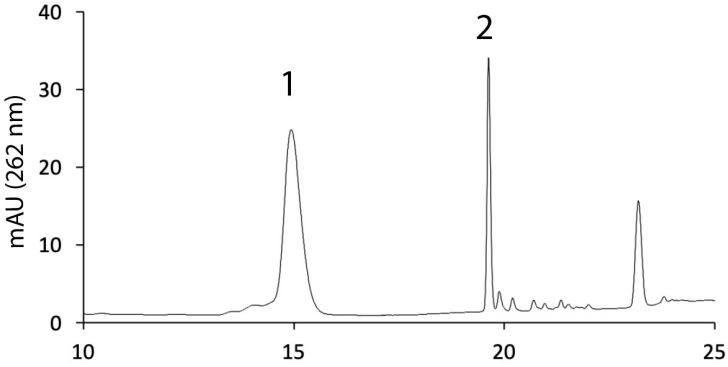

C JMV6 + p*lcpA* (ATc 50)

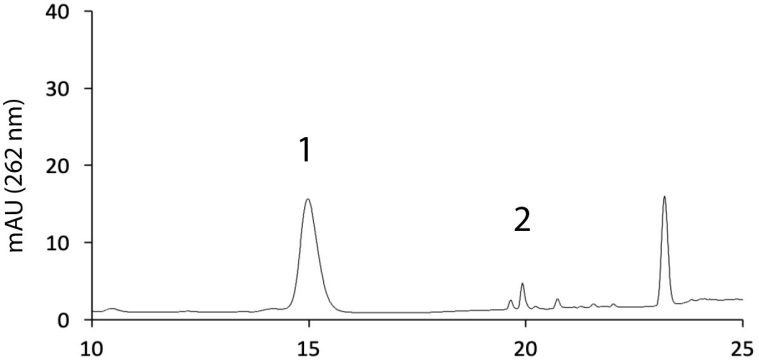

D

Strain	Peak	Retention Time (min)	Area (mAU*min)	Area/OD_{600nm}
JMV1	1	15.0	0.8	0.5
	2	ND	ND	ND
JMV6 (ATc 10)	1	14.9	11.5	10.65
	2	19.6	3.2	3.0
JMV6 + p*lcpA* (ATc 50)	1	15.0	6.9	3.0
	2	19.7	0.1	0.05

Peak 1 : UDP-Mur*N*Ac-pentapeptide Peak 2 : amidated UDP-Mur*N*Ac-pentapeptide

SUPPLEMENTARY DATA

Tables

Table S1: Primers used for plasmid constructions

Name	Use: Construction of …	5’ Primer tail	Primer
JV54	pJV4	GGCTACTGCCAGAGACC	GGAAAAGATCCGGGGGATCGATCCTCTAG
JV55		GGCTACTTGCTGAGACC	TTAGCCTAATTGAGAGAAGTTTCTATAG
JV50	pJV5	GCAGATAAATAA	TGCCAGAGACCGGAAAAGATCCGGG
JV51		GTGTAACTTTCC	TTGCTGAGACCTTAGCCTAATTGAGAGAAG
JV52		AAGGTCTCAGCAA	GGAAAGTTACACGTTACTAAAGGGAATG
JV53		AGCTTGCATGTCTGCAGGCCTCGAG	CTTGTCGGTAGCTGTGGTATGGATTG
TC287	pJV6		GTTTAAACTCCTTTTTGATAATCTC
TC288			CGCTTATAATCCATAACAATCATCC
TC289		TATGGATTATAAGC	GCCGAAGCAAACTTAAGAGTGTG
TC290		AAAAGGAGTTTAAAC	AAACACATTCCCTTTAGTAACGTG
JV48	pJV8	AGATTGTAGTTCTTCGGATCCTCTA	GACTATGGAACGTACACTTTTGGCG
JV49		CCGGTCTCTGGCA	TTATTTATCTGCGTAATCACTGTTTTTAGTC
JV58	pJV11 (*lcpA* deletion plasmid)	CGATAGGGTCTCGTTGC	GTCACCAAATACCATAGTTTCTT
JV59		CGATAGGGTCTCG	CATTAATATCCCCTACTTTCTAAATTTTTTAAT
JV60		CGATAGGGTCTCC	AATGGTATTTGAAAAAATTGATAAAAATAGT
JV61		CGATAGGGTCTCC	TAACTATTTATCAATTCCTGCAATTC
JV62		CGATAGGGTCTCG	GTTAAAAATTCCAAAACAAACCAATAATTTG
JV63		CGATAGGGTCTCG	TGCCTTAAGTCGCCCATTTTTAAAAC
JV64	pJV12 (*lcpB* deletion plasmid)	AGTACCGGTCTC	CTTGCCTATTGATAATAAAAATAAAAGTCTTAAGCT
JV65		AGTACCGGTCTC	CCATAAGTACCCCTTCTTTCTTCTT
JV66		AGTACCGGTCTCC	TATGGTATTTGAAAAAATTGATAAAAATAGT
JV67		AGTACCGGTCTCC	TAACTATTTATCAATTCCTGCAATTC
JV68		AGTACCGGTCTCC	GTTAAAAAATTCAACATAAAGTTTATTAAAAAGTATAAGA
JV69		AGTACCGGTCTC	CTGCCTTGATGGTATAACATCAACACC
JV70	pJV13 (*lcpAB* deletion plasmid)	TTCCTGGGTCTCCCC	TAATATCCCCTACTTTCTAAATTTTTTAAT
JV71		TTCCTGGGTCTCC	TAGGCCGGCCAAGTGGGCAA
JV72		TTCCTGGGTCTCCTTCT	TAGGGTAACAAAAAACACCGTATTTCTACGATGT
JV73		TTCCTGGGTCTCC	AGAAAATTCAACATAAAGTTTATTAAAAAGTATAAGATTAATTACT
TC381	pMEZ5		CTTTTTGATAATCTCATGACC
TC382			GAAATGCAAGTTTCTAACTAAC
TC383			TAGTTAGAAACTTGCATTTCACTTGCATTTCGGCCGGCCGAAGC
TC384			GTCATGAGATTATCAAAAAGACACATTCCCTTTAGTAACGTGTAACTTTC
TC403		GGCTACGGTCTCTTTGC	ACATTTCCTCCCCCAAATTATTAATTTATAATTATTTTTTATTAATTTTTATC

TC404	pMEZ12 (p*lcpA*)	GGCTACGGTCTCTTGCC	CTAATCTTCAACCATAATATCTTTAAATATGAAATC
JV101	pJV21 (p*lcpB*)	GGCTACGGTCTCA	TTGCTTTCTACTGAAAATGGTAGAAAAATAG
JV102		GGCTACGGTCTC	CTGCCTTATTGTTTAAACTCTATGTCATTAAATATAAAATC
JV136	pJV27 (insertion of P_{tet}-*lcpB* in the chromosome)	GGCTACGGTCTCTTGCC	TAAAAATAAGAAGCCTGCATTTGC
JV137		GGCTACGGTCTCT	TCCTTTACTGCAGGAGCTC
JV138		GGCTACGGTCTCTAGGAGAAAATT	TTTTGTCAAAATTAAAGAAATTTGTTATAC
JV139		GGCTACGGTCTCCTTGC	TTATTGTTTAAACTCTATGTCATTAAATATAAAATC

Table S2: primers used for PCR check of mutants

Name	Use : PCR check of …	Primer
JV85	*lcp* ORF replacement by c*atP* (JMV3, JMV4, and JMV6)	GCACTTTTCATCATTTCCACATCATTTAAC
JV86		GAATTTCATCATCAATAGGAAATTCAAATTGC
JV87		CAAATTCAGATACAGTAGTATTAGTAAATG
JV88		CTATACAAGATGATAGTATAAATACAGAGGC
JV90		GTACAAGGTACACTTGCAAAGTAGTGGTC
JV91		CAAGTTCATCACGCAGTATGTGACGG
JV99	P_{tet}-*lcpB* insertion in *erm* locus (JMV2 and JMV6)	GGCATGGCACATCAGTAAAAATTGAATAC
JV100		CGGTCACGGTGTAATCTTCTGTGACTGCC
TC153		GAATATTACTACCAAGAAAGCCAGTAG
TC154		GACATATTACACGATTTTATATTTAATGAC

Figures

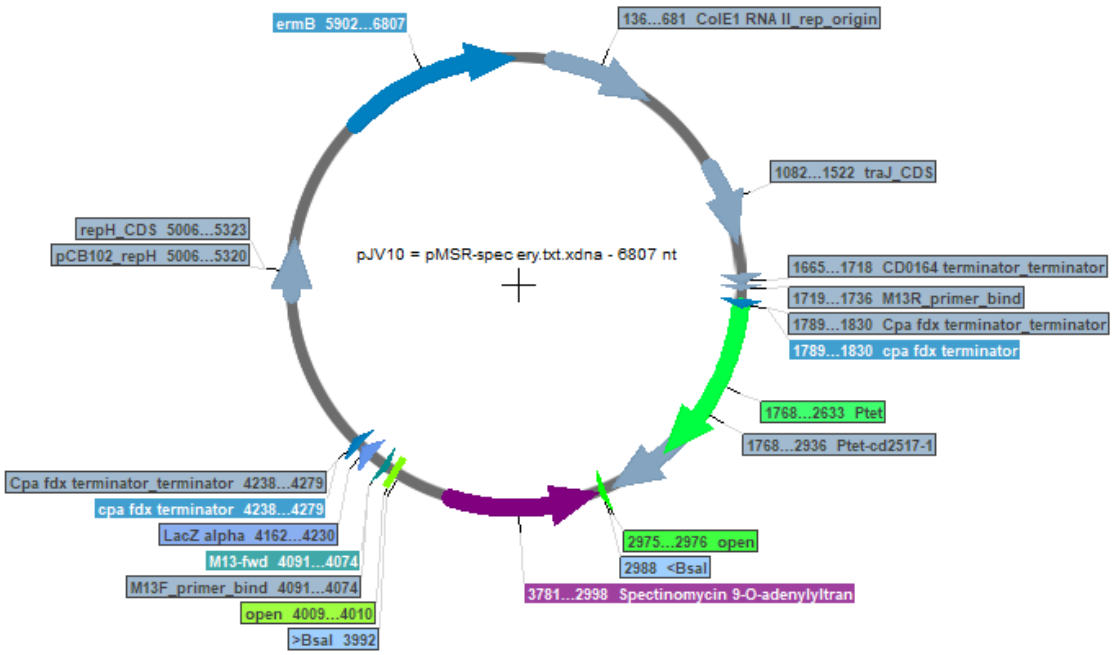

Figure S1

Graphic map of the pJV10 plasmid used to construct deletion plasmids of the *lcp*

On this graphic map of the pJV10 plasmid, created by Serial Cloner, the spectinomycin resistance gene flanked by BsaI sites to allow Golden Gate assembly, an erythromycin resistance gene, and the P_{tet}-CD2517 (Toxin) from the pMSR to facilitate counterselection during the allelic exchange are shown.

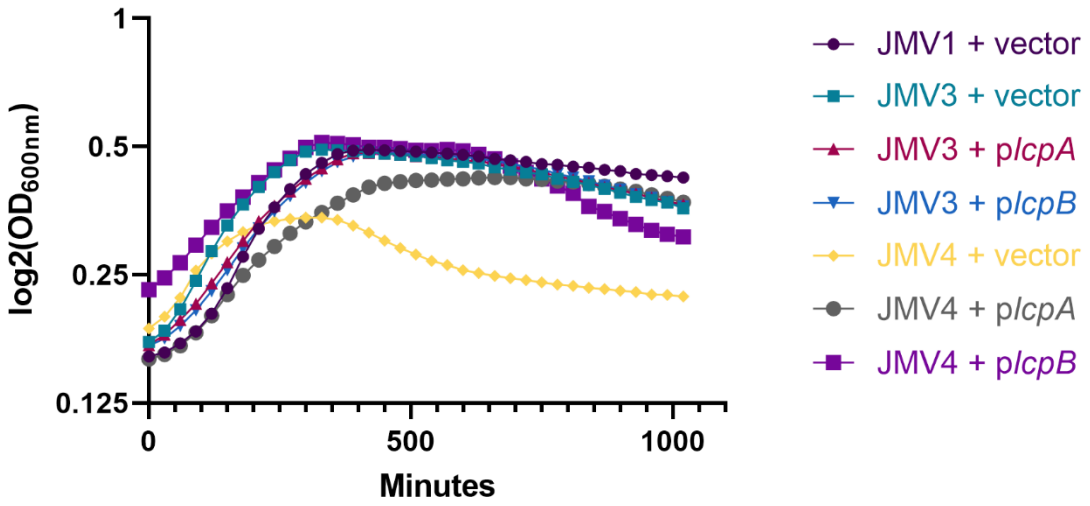

Figure S2

The Δ*lcpB* strain presents an altered growth

Growth curve of single mutant strains of *lcpA* (JMV3) *and lcpB* (JMV4), harboring either the pMTL84222, or the p*lcpA* or p*lcpB* plasmid. The growth was observed in BHI medium for 17 hours (1020 minutes). The graph represents the mean of 3 independent experiments.

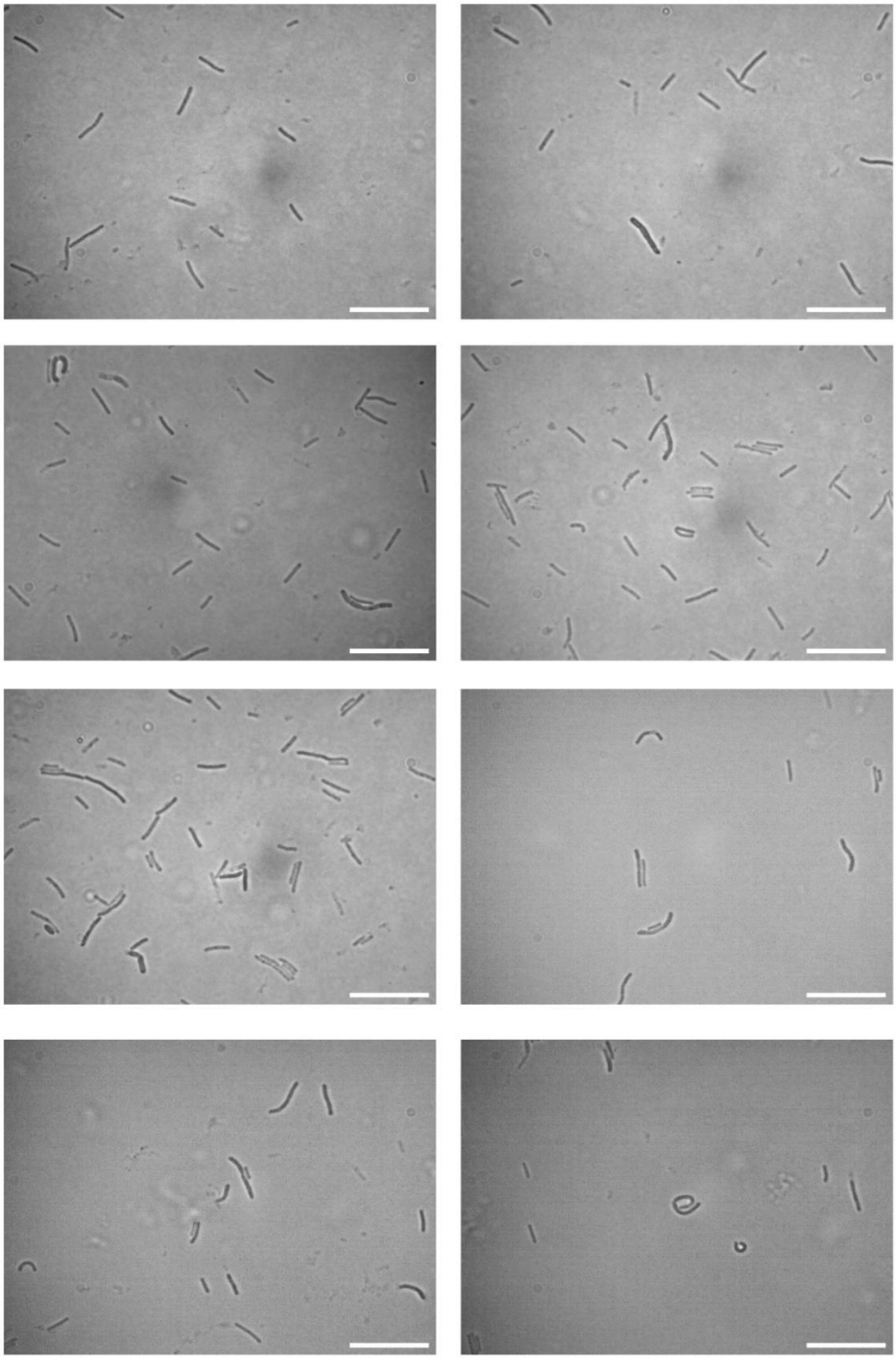

Figure S3

The Δ*lcpB* mutant (JMV4) is thicker, curved, or inflated in liquid culture.

These panels present additional pictures of the JMV4 strain observed in optic microscopy. The scale bar represents 20 µm.

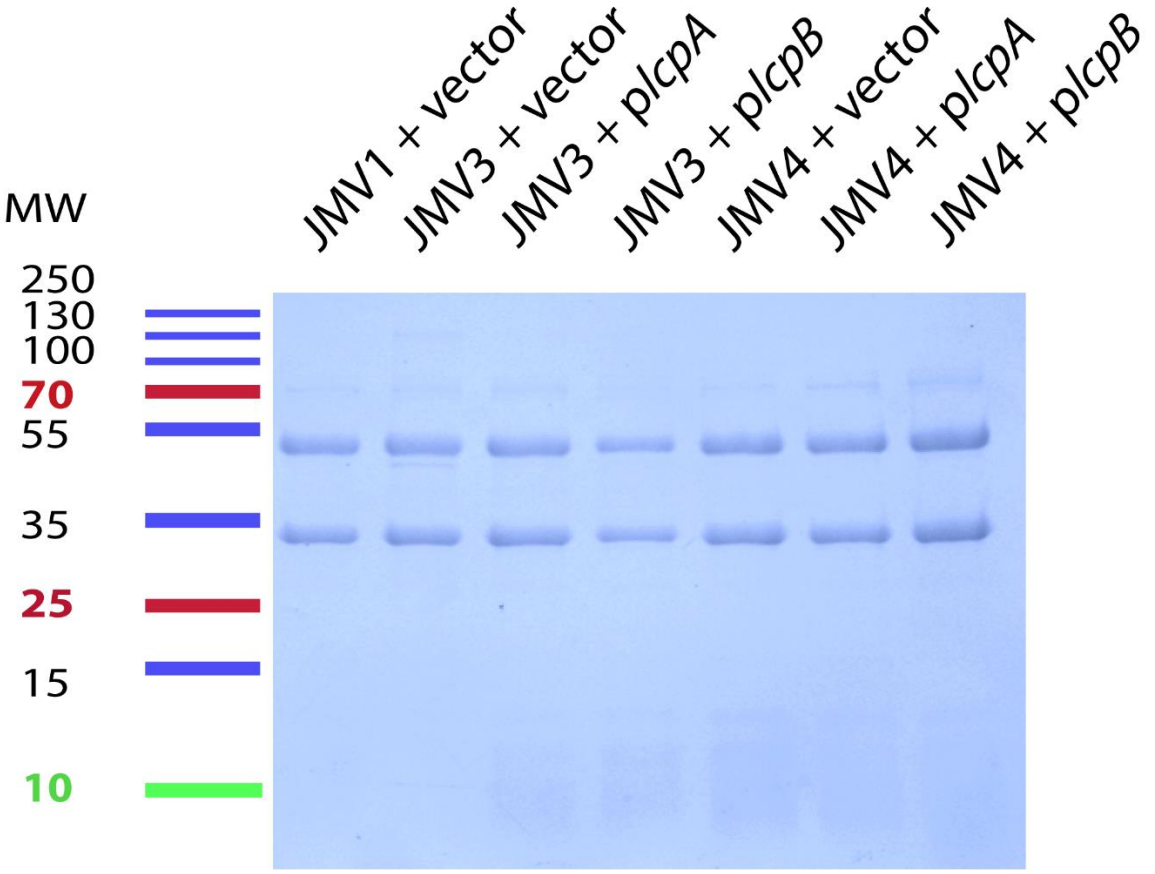

Figure S4

The single *Icp* mutants JMV3 and JMV4 exhibit a normal S-layer content

This Coomassie staining of Cwp protein extractions shows that the Cwp content of the S-layer of JMV1, JMV3 and JMV4 harboring either pMTL84222 (vector), p*IcpA* or p*IcpB* plasmid. The protein ladder is graduated in kg Dalton (kDa). MW: molecular weight.

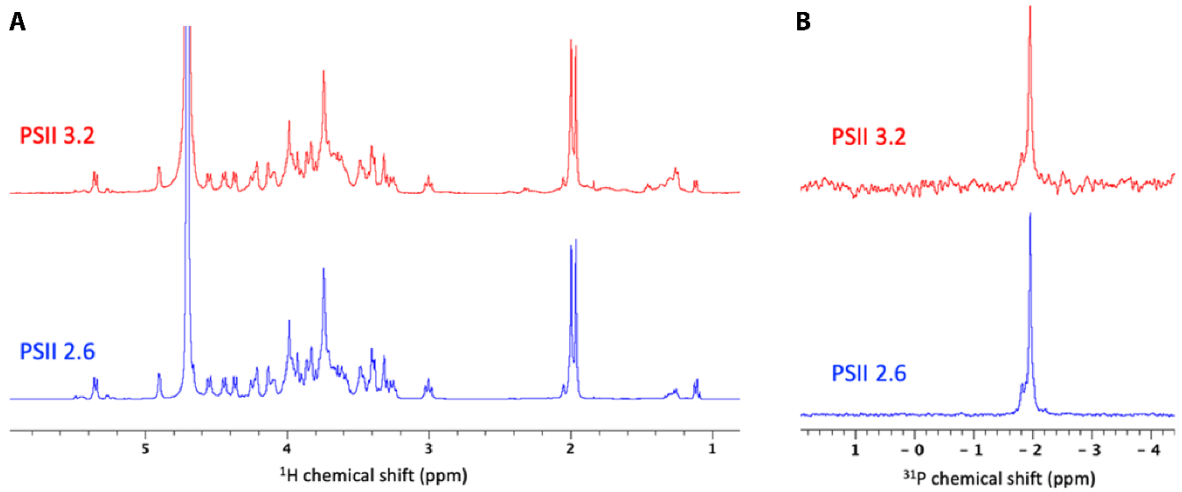

Figure S5

The PSII was obtained and the absence of contamination with LTA was confirmed by NMR.

^{1}H (**A**) and ^{31}P (**B**) NMR spectra of the PSII extracted from culture pellets of the 630 strain. Two samples were sent for analysis, named PSII 3.2 and PSII 2.6. Both were confirmed to contain PSII. The chemical shift is measured in part-per-million (ppm).

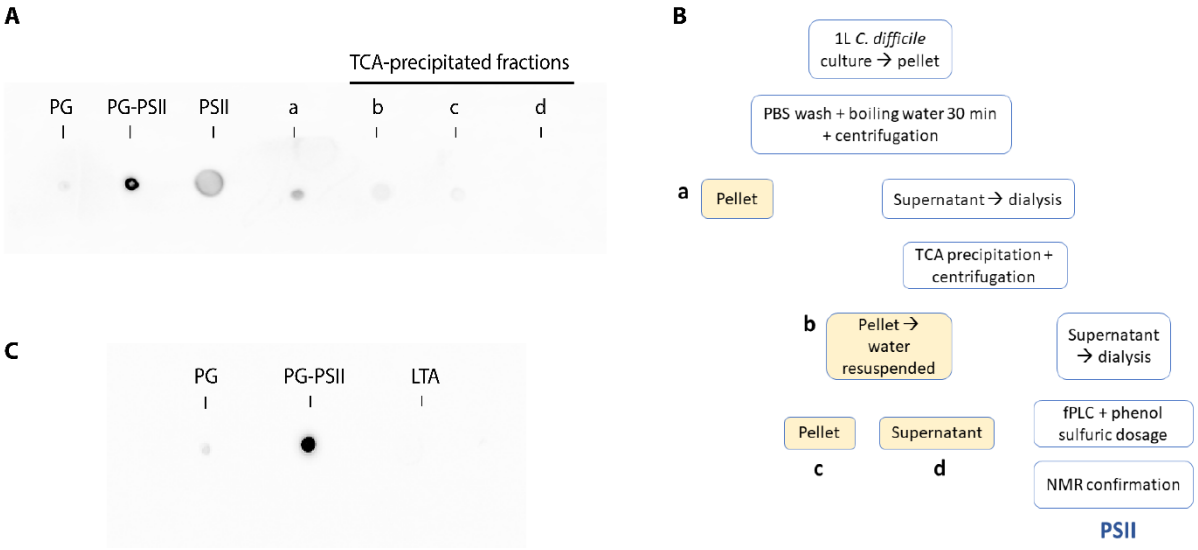

Figure S6

The immunization led to antibodies production and these antibodies showed good specificity for the PSII

This dot blot assay shows that the antibodies produced by the rabbits recognize well the RMN-verified PSII (**A**) of *C. difficile* and the PG linked PSII (PG-PSII) (**A** and **C**) and do not cross-react with peptidoglycan (**A** and **C**) or lipoteichoic acid (LTA) (**C**) of *C. difficile*. Moreover, different samples at different stages of the purification process were tested (**B**). Briefly, PSII purification protocol was performed as followed (white boxes, steps of PSII purification, yellow boxes, potential contaminant molecules) : 1 litter of *C. difficile* culture was pelleted. Pellet was washed in PBS and boiled in water for 30 minutes. After centrifugation, pellet (a) was tested to know whether some PSII were not recovered. The supernatant was further used for purification and a TCA precipitation was performed. After centrifugation, pellet (b) was tested to know whether some PSII was not recovered; it was resuspended in water and centrifuged again, giving pellet (c). The supernatant (d) was dialyzed and applied on fPLC. PSII was recovered, dosage was performed by phenol sulfuric method and PSII was analyzed by NMR.

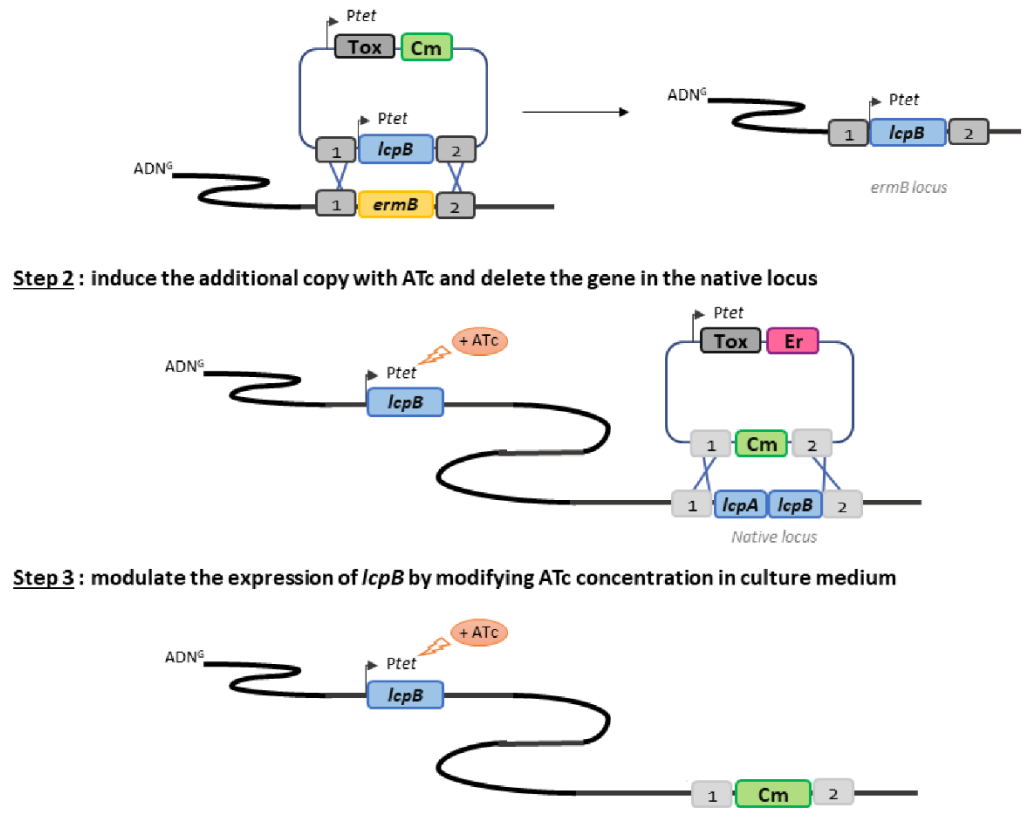

Figure S7

A new strategy designed to construct a conditional-lethal mutant in *C. difficile*

Schematic representation of the strategy used to create a conditional-lethal mutant of *C. difficile lcpA* and *lcpB* genes. The strategy consists in three major steps: first the insertion of an inducible copy of *lcpB* in the *erm* locus of the chromosome (under control of P_{tet}), then the deletion of both *lcpA* and *lcpB* by replacing the ORFs with a *catP* gene, and finally the control of the *l* expression of *lcpB* thanks to ATc induction.

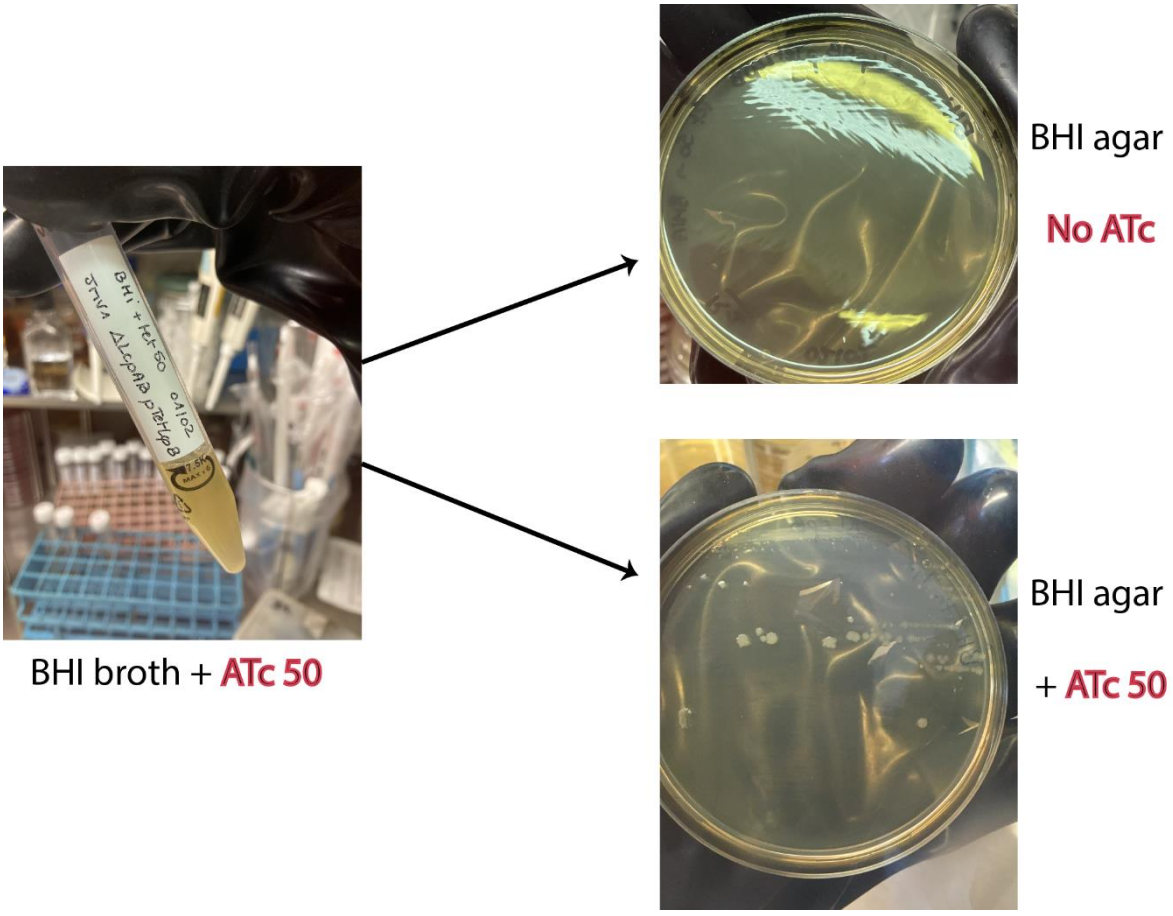

Figure S8

The anchoring of PSII is essential for *C. difficile* growth

The conditional-lethal mutant pre-cultured overnight in liquid BHI in the presence of 50 ng.mL^{-1}ATc is not able to grow on a BHI plate without ATc but grows correctly in the presence of ATc at 50 ng.mL^{-1}.

Texts

Text S1: construction of plasmids for the study

The plasmids used in this study were constructed using either the Gibson assembly protocol from NEB (23) or the Golden Gate assembly from NEB (24, 25) cloning technique. For Golden Gate assembly, the primers were designed using the NEB Builder® assembly tool.

Construction of deletion plasmid for the *ermB* locus

pJV4: the spectinomycin cassette was amplified from pAT28 and flanked with BsaI sites using JV54/JV55 primers. The PCR product was inserted in the pBLUNT cloning vector by blunt-end DNA cloning to give pJV4.

pJV5: the spectinomycin cassette flanked with BsaI sites was amplified from pAT28 using JV50/JV51 primers, and the downstream region of *ermB* locus was amplified from genomic DNA of 630 strain using JV52/53 primers. Both PCR products were assembled using the Gibson assembly protocol (NEB Biolabs) to give pJV5.

pJV7: the spectinomycin cassette flanked with BsaI sites was extracted from pJV4 using restriction digestion with XhoI and BamHI. The pMSR was opened by restriction digestion with XhoI and BamHI. The spectinomycin cassette was then cloned into the linearized pMSR plasmid by a classical ligation process.

pJV8: the upstream region of the *ermB* locus was amplified from genomic DNA of 630 strain using JV48/JV49 primers, and the spectinomycin + downstream region of *ermB* locus fragment was amplified from pJV5 using JV50/JV53 primers, and the pMSR plasmid was amplified using JV46/JV47 primers. The three PCR products were assembled using the Gibson assembly protocol (NEB Biolabs) to give pJV8.

Constructing deletion plasmids for *lcpA*, *lcpB* and the conditional-lethal deletion of both *lcp*

pJV6: the *ermB* cassette was amplified from pMTL84222 using TC289/TC290 primers, and pMTL83151 was amplified using TC287/TC288 primers. Both PCR products were assembled using the Gibson assembly protocol (NEB Biolabs) to give pJV6. pJV10: this plasmid results from the subcloning of pJV7 (fragment with the spectinomycin resistance cassette flanked by BsaI sites and P_{tet}-CD2517 toxin) into pJV6 (Erm^R) using the restriction enzymes SacII and XhoI.

pJV11: the upstream and downstream regions of *lcpA* were amplified from genomic DNA of 630 strain using respectively JV58/59 and JV62/JV63 primers. The *catP* cassette was amplified from the pMSR plasmid using JV60/JV61 primers. The three PCR products were inserted in the pJV10 using the Golden Gate assembly protocol (NEB Biolabs) to give pJV11.

pJV12: the upstream and downstreamregions of *lcpB* were amplified from genomic DNA of 630 strain using respectively JV64/65 and JV68/JV69 primers. The *catP* cassette was amplified from the pMSR plasmid using JV66/JV67 primers. The three PCR products were inserted in the pJV10 using the Golden Gate assembly protocol (NEB Biolabs) to give pJV11.

pJV13: the upstream region of *lcpA* and the downstream region of *lcpB* were amplified from genomic DNA of 630 strain using respectively JV58/JV70 and JV73/JV69 primers. The *catP* cassette was amplified with its promoter from the pMSR plasmid using JV71/JV72 primers. The three PCR products were inserted in the pJV10 using the Golden Gate assembly protocol (NEB Biolabs) to give pJV11.

Constructing complementation plasmids for *lcpA* and *lcpB*

pTC131: pJV4 was digested using BamHI/XhoI restriction enzymes, and the DNA fragment Spec of approximately 1kb was ligated pMTL84151 previously digested by BamHI/XhoI restriction enzymes.

pMEZ5: The *ermB* cassette from pMTL-84222 was amplified using TC383/TC384 primers, and pTC131 was amplified using TC381 and TC382 primers. Both PCR products were assembled using the Gibson assembly protocol (NEB Biolabs) to give pMEZ5.

pMEZ12: P_{lcpA}-*lcpA* was amplified from genomic DNA of 630 strain using TC403/TC404 primers and inserted in pMEZ5 using the Golden Gate assembly protocol (NEB Biolabs) to give pMEZ12.

pJV20: P_{lcpB}-*lcpB* was amplified from genomic DNA of 630 strain using JV101/JV102 and inserted in pTC131 using the Golden Gate assembly protocol (NEB Biolabs) to give pJV20.

pJV21: pJV20 was digested using StuI and KpnI restriction enzymes, and the DNA fragment of approximately 1,5kb was ligated with pMTL84222 (Erm^R) previously digested by StuI and KpnI restriction enzymes.

pJV27: the P_{tet} was amplified from pRPF185 using JV136/JV137 primers, and the *lcpB* was amplified from genomic DNA of 630 strain using JV138/JV139 primers. Both PCR products were inserted in pJV8 using the Gibson assembly protocol (NEB Biolabs) to give pJV27.

Cloning *gusA* reporter plasmids

pMDR1: Kanamycin cassette flanked with BsmBI restriction enzyme sites was amplified from pJV4 using TC393/TC394 primers. *gusA* was amplified from pRPF185 using TC395/TC396 primers. Both PCR DNA fragments were inserted into pTC131 using the Golden Gate assembly protocol to give pMDR1.

pMDR2: Spectinomycin cassette was amplified from pAT28 using TC397/TC398 and inserted into pMDR1 to give pMDR2.

pMDR8: P_{lcpA} was amplified from genomic DNA of 630 strain using TC409/TC410 and inserted into pMDR2 to give pMDR8. P_{lcpB} was amplified from genomic DNA of 630 strain using TC411/TC412 and inserted into pMDR2 to give pMDR5.